Collection of Heat Loss in Photovoltaic System by Parallelly Connected Thermoelectric Network

A THESIS SUBMITTED TO THE FACULTY OF THE UNIVERSITY OF MINNESOTA BY

Joel Daniel Erickson

IN PARTIAL FULFILLMENT OF THE REQUIREMENTS FOR THE DEGREE OF MASTER OF SCIENCE IN ELECTRICAL ENGINEERING

June 2022

Acknowledgements

Thank you to my research advisor Jing Bai for your support and guidance with this project. Thank you to my additional committee members Mohammed Hasan and Zhihua Xu for your time and input. And thank you to the entire UMD EE department for supporting my education and all I have learned from you.

Abstract—The goal of this work is to increase solar cell efficiency by efficiently combining the electric power of a solar cell and a thermoelectric generator into a single two terminal hybrid device. This work presents a method of achieving this by dividing the thermoelectric generator into smaller thermoelectric generators, forming a parallelly connected network with them, and connecting this network in series with the solar cell. An equivalent circuit model was developed for this device scheme and compared with experimental data. The data show some support of the model, but fine evaluation of the model's accuracy was hindered by limitations in the experimental setup. If thermoelectric generator efficiency increases in the future, it may become practical to combine thermoelectric generators with solar cells. Providing a method for combining the two power sources at the cellular level may be important for simplifying and improving systems that use these photovoltaic/thermoelectric hybrids.

Table of Contents

List of Tables

List of Figures

Chapter 1: Introduction

Chapter 1 presents a brief background of hybridizing thermoelectric generators with photovoltaics as well as brief discussion of prior research on the topic of electrical combination of the two elements. The specific content of this work is also introduced and a chapter outline presented.

1.1 Background

In single junction solar cells, nearly half of the incident sunlight's energy is lost as waste heat [19]. This occurs because of the spectral mismatch between the incident photons and the energy bandgap of the solar cell material. When photons have more energy than the bandgap, the extra energy is converted into waste heat rather than contributing to the photoelectric effect. When photons have a lower energy, they do not contribute to the photoelectric effect and can produce waste heat. The conversion of sunlight into waste heat results in a lower energy conversion efficiency for the solar cell and can contribute to a degradation in performance due to the increased operating temperature [19].

One method of recovering some of the energy from this waste heat is to combine a thermoelectric generator (TEG) with the photovoltaic (PV) element. The waste heat is used to produce a temperature gradient across the TEG that produces a voltage difference due to the Seebeck effect. Many variations of this approach have been devised and a large amount of research is going into the development of PV/TEG hybrid devices [12, 14, 16, 20].

Currently, TEGs have a relatively low energy conversion efficiency due to the lack of thermoelectric materials with the necessary material characteristics. As a result, PV/TEG hybrid devices are not used outside of research. However, significant research has been put into improving TEG devices, as well as developing better thermoelectric materials [4, 6, 17, 20]. This means that high efficiency TEGs, along with practical PV/TEG hybrid devices, may be available in the near future.

In most PV/TEG hybrid research, the PV element and the TEG are kept electrically separate with each acting as an independent electrical power source [14, 16, 20]. Electrically combining the PV element and TEG to produce a two terminal hybrid device with its own current voltage (IV) curve has a number of benefits. These include simplification of the system as well as reducing the number of power electronics and other supporting equipment needed for each power source in the system.

1.2 Current State of Electrically Combined PV/TEG Hybrids

Some PV/TEG hybrid devices with electrical combination have been created in research, but little investigation into the electrical combination aspect has been performed [22, 23]. The two basic connection methods are a series connection or a parallel connection. In prior research, it seems that the series connection is the most useful [7, 12, 13]. The series connection presents two main issues. One is that the TEG resistance adds to the series resistance of the PV element and degrades the fill factor of the hybrid

device's IV curve [12]. The second issue is that mismatch between the PV element current and TEG current can have undesirable effects [9, 21].

Ideally, there would be some way to electrically combine the PV element and TEG such that the hybrid device had a max power equal to the PV element max power plus the TEG max power. A way to do this has been presented in prior research, but it is not practical to implement in real world applications [13]. In this method, the temperature gradient across the TEG needs to be increased to some optimal value where the hybrid device's max power is a lossless combination of the PV element and TEG max power. This would require a separate energy source to either heat the hot side of the TEG or cool the cold side of the TEG.

1.3 Solution Presented in This Work

In this work, a new method of electrically combining the PV element and TEG power is presented. In this method, the TEG is electrically divided into sub-TEGs by changing the number of TEG leg pairs that are connected in series. The sub-TEGs are then parallelly connected to form a TEG network that is connected in series with the PV element.

This method offers two primary benefits. The first benefit is that the series resistance introduced by the TEG is reduced due to the splitting as well as the sub-TEGs being in parallel. The second benefit is that the PV element's current is divided amongst the sub-TEGs, which will make it more closely match the TEG current.

The goal of this work is to investigate the efficacy and potential problems of this connection method. To do this, a circuit model of the PV/TEG series connected hybrid with TEG splitting was developed based on the PV/TEG series connected circuit model that has been presented in prior research [7, 13]. The behavior of this model was examined empirically. Also, an experimental device with TEG splitting was created and measurements were taken to test the accuracy of the circuit model.

1.4 Outline of Thesis Chapters

Chapter 2 is a literature review of past research done on relevant topics. Chapter 3 is a collection of background theory relevant to the work. Chapter 4 covers the circuit model and investigation of its behavior. Chapter 5 covers the experimental investigation of the circuit model. Chapter 6 is a conclusion that discusses the results of chapters 4 and 5, as well as suggestions for future research.

Chapter 2: Literature Review

Chapter 2 presents a brief history of thermoelectric devices and the current state of research on thermoelectric/photovoltaic hybrid devices. Individual works on the electrical combination of the two elements are also discussed in more detail.

2.1 Brief History of Thermoelectric Devices [3, 8]

In 1822, Thomas Seebeck discovered the first of the thermoelectric effects by showing that a junction of two different metals produced a voltage difference when subjected to a temperature gradient. Soon after, Jean Peltier showed that the inverse of this effect also occurred for a junction of two different materials. In the middle of the nineteenth century, William Thomson produced an explanation for the two prior thermoelectric effects and derived a set of expressions, known as the Kelvin relations, that showed how the two effects were related to each other. He also predicted the existence of the third thermoelectric effect, which applies to a single material.

Shortly after the discovery of the Seebeck and Peltier effects, people began trying to make devices that exploited the effects to generate voltage or cooling/heating. Progress in increasing thermoelectric device efficiency was quite slow at first. In the middle of the twentieth century, semiconductor technology began to rapidly advance and more efficient thermoelectric devices were made. However, device efficiencies were still considerably low. Thermoelectric devices were confined to very niche applications where the need for reliability and low maintenance far outweighed the need for efficient energy conversion.

The intervention of semiconductors made thermoelectric materials with figures of merit around 1 achievable. From here to the beginning of the twenty-first century, progress in thermoelectric device efficiency again saw a phase of stagnation. But this has recently changed. Over the last ten years, research has been producing thermoelectric materials with figures of merit greater than 1 [11]. Much of this recent progress has been achieved through the development and implementation of nanotechnology [11].

2.2 Combining Thermoelectric Devices with Photovoltaic Devices

Several different approaches to combining thermoelectric generators (TEGs) with photovoltaic (PV) devices to utilize waste heat have been explored [12, 14, 16]. In thermally coupled hybrid devices, the heat being utilized by the TEG is coming from the PV element. In this scheme, the temperature gradient applied to the TEG is related to the temperature of the PV element. Increasing the temperature gradient applied to the TEG increases the voltage it generates, but also increases the temperature of the PV element. Since solar cell performance tends to degrade with increasing temperature, this presents conflict between the power produced by the TEG and that produced by the PV element making optimization of these devices complicated.

Another approach is optically coupled hybrid devices. In these devices, solar radiation that is not efficiently converted to electrical energy by the PV element is directed to the TEG to heat up one side and generate a temperature gradient. The PV element and TEG are kept thermally separate, which has the advantage of keeping the PV element temperature independent of the TEG's temperature gradient. However, separating and directing parts of the solar radiation spectrum to the PV element and TEG separately adds its own complications to the system.

Many variations of these two methods exist with the addition of system modifications [12, 14, 16]. These include things like adding heat sinks to the TEGs, adding materials with certain thermal properties between the PV element and TEG, transferring thermal energy with fluids or other methods, and many other methods.

In addition, the choice of whether to keep the TEG and PV element electrically separate or combined increases the choices of hybrid device schemes. In the current literature, most hybrid devices keep the TEG and PV element electrically separated and research on their electrical combination is scarce.

Currently, there is only one book on the subject of PV/TEG hybrid devices by Narducci et al [12]. In the book, there is a brief mention of electrical combination of the TEG and PV element power. It is explained that connecting the TEG in series to the PV element will increase the open circuit voltage while a parallel connection will increase the short circuit current. The book also discusses the problems associated with mismatch between the TEG series resistance and the internal resistances of the PV element. If the TEG is series connected and the TEG series resistance is much larger than the PV element's series resistance, the fill factor of the IV curve is degraded and the hybrid device will have a low output power. If the TEG is parallelly connected and the TEG series resistance is much smaller than the PV element's shunt resistance, the fill factor will again be degraded.

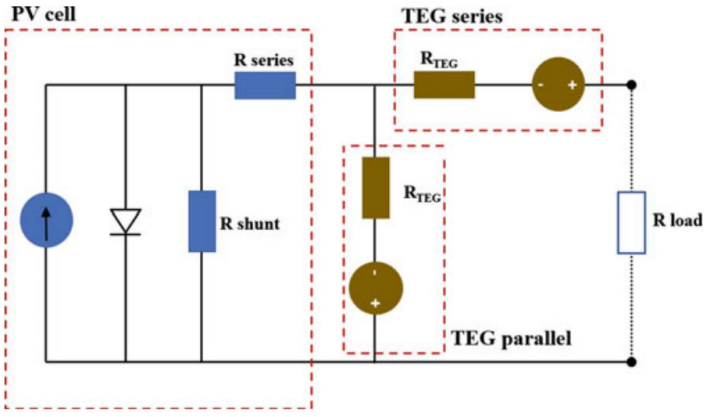

***Figure 2.1**: PV/TEG hybrid device electrical connection methods presented in [12].*

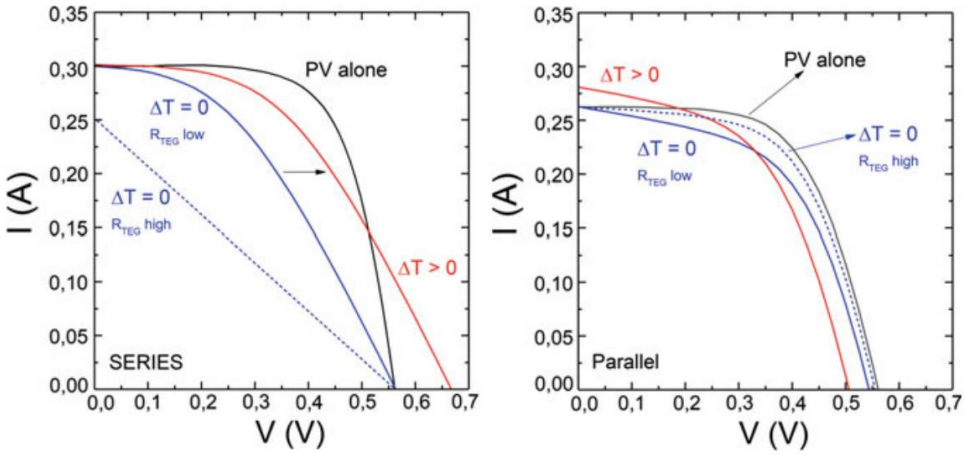

Figure 2.2: *Effects of resistance mismatch in electrically combined PV/TEG hybrid presented in [12].*

2.3 Prior Research on Electrically Combined PV/TEG Hybrid Devices

Two papers were found that made electrically connected hybrid devices [22, 23]. In the first paper, a dye sensitized solar cell was thermally coupled and combined in series with a TEG to make a hybrid device. In the second paper, a perovskite solar cell was thermally coupled and combined in series with a TEG to make a hybrid device. Both devices used ice water to cool the cold side of the TEG and resulted in hybrid devices that had increased max power compared to the solar cells by themselves. However, neither paper compared the hybrid max power to the sum of the PV element power and TEG power nor did any other type of investigation into the electrical connection aspect of the devices.

Three papers were found that specifically investigated electrical combination of the TEG and PV element in PV/TEG hybrid devices. In the first paper, the series connection of the TEG and PV element was compared with the parallel connection [25]. A computer model of the hybrid device with a boost converter that tracked the max power was developed. The transient response of the device power with either the series or parallel connection was modeled for different types of change in solar radiation. These included slow change, step change, and ramp change.

The model showed that for conditions where the device temperature is constant while the solar radiation varies, such as for the step change, the parallel connection produces greater power. For conditions where the temperature increases linearly with solar radiation, such as with a slow change, the series connection produces greater power. The model for each test was compared with experimental results by simulating a TEG/PV hybrid using power supply and load devices. The experimental results agreed with the results of the model. This study compared the parallel connection with the series connection but did not investigate how the hybrid device power compared with the powers of the TEG and PV element by themselves.

Because of this, it's not clear if the hybrid devices in this study were producing more or less power than the PV element alone.

In the second paper, a method for lossless electrical combination of the TEG and PV element was presented for the series connection [13]. First, a circuit model of the hybrid device was presented by combining the single diode circuit model of a solar cell in series with the circuit model of a TEG.

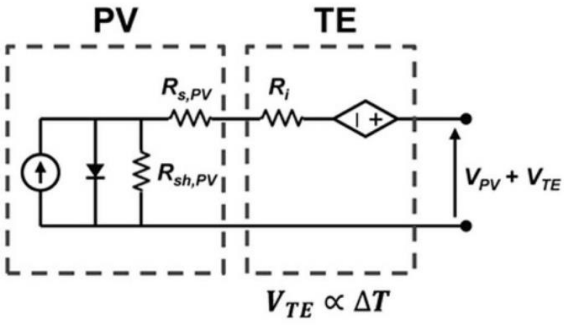

Figure 2.3: *Circuit model of series connected PV/TEG hybrid presented in [13].*

By summing the currents in each branch of the circuit model, an equation for the current voltage relationship of the hybrid device was developed. The photo current of the solar cell (I_L) is shown as the current source on the left side of the circuit model. The diode is modeled by Shockley's diode equation where I_0 is the reverse saturation current, V_T is the thermal voltage, which is equal to Boltzmann's constant multiplied by the solar cell temperature and divided by the charge of an electron ($k_B T/q$), and n is the diode ideality factor. The open circuit voltage of the TEG is V_{TEG}, which is represented by the diamond shaped voltage source in the circuit model. The resistance of the TEG is R_{TEG}, which is shown as R_i in the circuit model. R_s is the series resistance of the solar cell, R_{sh} is the shunt resistance of the solar cell, V is the voltage across the load (shown as $V_{PV} + V_{TE}$ in the circuit model), and I is the current through the load.

$$I = I_L - I_0\left[e^{\frac{V+V_{TEG}+I(R_s+R_{TEG})}{nV_T}} - 1\right] - \frac{V+V_{TEG}+I(R_s+R_{TEG})}{R_{sh}} \tag{2.1}$$

Numerical methods were used to model this equation, and the difference between the hybrid device power and the sum of the PV and TEG powers was found as a function of the TEG resistance and the TEG voltage. Zero difference between the hybrid device power and the sum of the TEG and PV powers, or lossless hybridization, was found to correspond to a straight line in the TEG resistance and TEG voltage plane. This means that whatever the value of the TEG resistance, the hybrid device can be made electrically lossless by making the TEG voltage some optimal value. Since the TEG voltage is determined by the

temperature gradient applied to it, the lossless power combination is achieved by applying the proper temperature gradient to the TEG. An experimental setup was included that verified this result.

The third paper is essentially a continuation of the work in the previous paper [7]. In this paper, the same circuit model of the hybrid device from paper two was used. The ratio of the series connected PV/TEG hybrid power to the PV power alone at room temperature (G_p) was compared with the point of lossless power combination in the hybrid. How the TEG voltage, TEG resistance, and solar cell series resistance affected when $G_p = 1$ and the lossless condition coincided was studied.

It was found that the smaller the PV series resistance, the smaller the TEG voltage needed to be to achieve the lossless condition and the TEG voltage needed to achieve the lossless condition increased linearly with the TEG resistance. It was also found that the lossless condition did not always correspond to $G_p = 1$. When the ratio of the TEG resistance to the PV series resistance increased, the value of G_p at the lossless condition also increased. Also, the lossless condition occurs for a specific value of the TEG voltage, so increasing past this voltage leads back to electrical losses. This paper also included an experimental setup that supported the results of the model.

Although a method for lossless electrical combination of the TEG and PV element was presented in this previous work, it is not that useful. The method presented requires controlling the temperature gradient applied to the TEG in order to achieve the lossless condition. Since the temperature gradient across the TEG is determined by the waste heat produced by the solar cell, controlling it would require either adding or removing heat to the system with some additional power source, which is not practical for the application in mind.

Chapter 3 Background Theory

Chapter 3 presents a collection of background theory on thermoelectric materials, thermoelectric devices, photovoltaic devices, and thermoelectric/photovoltaic hybrids.

3.1 Thermoelectric Effects [3, 11, 12]

Thermoelectric phenomena are governed by several closely related effects. The Seebeck effect is the development of a voltage difference between the ends of a junction of two dissimilar materials when the junction and the material ends are at different temperatures. This occurs because the temperature difference causes charge carriers (typically electrons or holes) to concentrate towards the cooler end. The imbalance of electrons between the two cool ends of the junction produces a voltage difference. The voltage produced by this effect is proportional to the temperature difference applied to the junction by a constant known as the Seebeck coefficient.

$$V = \alpha_{AB} \Delta T \tag{3.1}$$

In the above expression, V is the voltage, ΔT is the temperature difference, and α_{AB} is the Seebeck coefficient of material A minus the Seebeck coefficient of material B.

When a current is applied to a junction of two dissimilar materials, a temperature difference develops between the junction and the two ends, known as the Peltier effect. This happens because the electrons move to higher or lower energy states as they pass from material A to material B. In order to make this change, the electrons either absorb or release energy in the form of heat causing one end to cool and the other to heat up. The rate of heating or cooling at each end is proportional to the current by a constant known as the Peltier coefficient.

$$Q = \pi_{AB} I \tag{3.2}$$

In the above expression, Q is the heating or cooling at each end, I is the current, and π_{AB} is the Peltier coefficient of material A minus the Peltier coefficient of material B.

The third thermoelectric effect is the Thomson effect. This effect occurs in a homogenous conduction and manifests as reversible heating (different from joule heating) or cooling when an electric current and a temperature gradient are applied to the conduction. This effect also has a related coefficient known as the Thomson coefficient. It is defined as the rate of heating per unit length when a unit current is run through the conductor subject to a unit temperature gradient.

The three thermoelectric effects are related by two relations known as the Kelvin relations. In the first relation, the Peltier coefficient is equal to the Seebeck coefficient multiplied by the temperature.

$$\pi_{AB} = \alpha_{AB} T \tag{3.3}$$

The second Kelvin relation relates the Thomson coefficient to the change in Seebeck coefficient with respect to temperature.

$$\tau_A - \tau_B = T\frac{\partial \alpha_{AB}}{\partial T} \tag{3.4}$$

In the above expression, τ_A is the Thomson coefficient of material A and τ_B is the Thomson coefficient of material B.

One thing to point out is that the Seebeck and Peltier effects require a junction between two different materials, and the coefficients in (3.1) and (3.2) are the difference in either Peltier or Seebeck coefficients between materials A and B. The Seebeck or Peltier coefficient of a superconductor is zero, so the coefficient of a different material can be found by measuring the corresponding thermoelectric effect when in a junction with a superconductor at the superconducting temperature. The coefficients of the non-superconductor material can then be found at higher temperatures by using the Kelvin relations. All three coefficients can be temperature and spatially dependent in complicated ways, depending on the physical characteristics of the thermoelectric materials being used.

3.2 Transport Coefficients [11]

In general, a thermoelectric material may have a temperature gradient across it as well as current from some other electromotive force. The total electric current density in the material can be described with the following.

$$J = \sigma\mathcal{E} - \sigma\alpha\frac{\partial T}{\partial x} \tag{3.5}$$

In the above relation, J is the current density, σ is the electrical conductivity coefficient, $\mathcal{E}$ is the total electromotive force, α is the Seebeck coefficient, and $\frac{\partial T}{\partial x}$ is the temperature gradient. The total heat current density in the material can be described with the following.

$$J_Q = \pi\sigma\mathcal{E} - \kappa\frac{\partial T}{\partial x} \tag{3.6}$$

In the above expression, J_Q is the heat current density, π is the Peltier coefficient, and κ is the thermal conductivity coefficient. The thermal conductivity coefficient can be thought of as the sum of the lattice thermal conductivity κ_L and the electronic thermal conductivity κ_e. The lattice thermal conductivity describes how well heat is transported by phonons in the material lattice while the electronic thermal conductivity describes how well heat is transported by charge carriers in the material.

Mathematical expressions of these coefficients in relation to fundamental material characteristics can be derived from the Boltzmann transport equation or the Landauer approach. With some approximations, the expression for the conductivity coefficient when electrons and holes are the charge carriers is found to be

$$\sigma = \int_{-\infty}^{\infty} \frac{2q^2}{h} \lambda(E) \frac{M(E)}{A} \left(-\frac{\partial f_0}{\partial E}\right) dE \tag{3.7}$$

where q is the charge of an electron, h is Plank's constant, λ(E) is the charge carrier mean free path (as a function of energy), M(E) is the number of transport channels (as a function of energy), A is the cross-sectional area of the material, and $\frac{\partial f_0}{\partial E}$ is the derivative of the Fermi function with respect to energy. For materials that have the conduction band lower or higher than the Fermi level (i.e., degenerate semiconductors and lightly doped semiconductors), the conductivity coefficient is low. For materials that have the Fermi level located within the conduction band (i.e., heavily doped semiconductors and metals), the conductivity is high and increases as the Fermi level is pushed deeper into the conduction band.

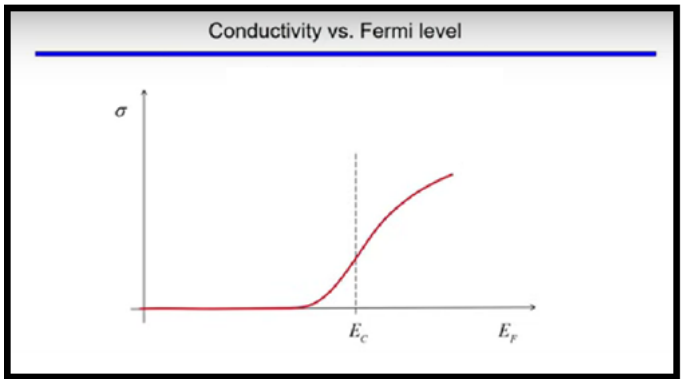

Figure 3.1*: Conductivity vs Fermi level. The horizontal axis is the Fermi level and the vertical axis is the conductivity. The dotted line labeled E_c is the point where the Fermi level is at the edge of the conduction band. Adapted from [11].*

The expression for the Seebeck coefficient is shown below.

$$\alpha = -\frac{1}{qT}(E_J - E_F) \tag{3.8}$$

E_J is the average energy at which current flows and E_f is the Fermi level. The average energy at which current flows will be somewhere in the conduction band of the material. When the Fermi level is lower or higher than the conduction band, $E_J - E_F$ is large and the Seebeck coefficient of the material will be large. When the Fermi level is in the conduction band, $E_J \approx E_F$ making $E_J - E_F$ small and thus the Seebeck coefficient small. This is why metals and heavily doped semiconductors have such weak thermoelectric effects. Their Fermi level is inside the conduction band resulting in a higher conductivity coefficient but a low Seebeck coefficient. Also, notice that when the conduction band is above the Fermi level (the case for an n type semiconductor) $E_J - E_F$ will be positive and the Seebeck coefficient will be negative. In a p type semiconductor, the conduction band is below the Fermi level and the Seebeck coefficient will be positive.

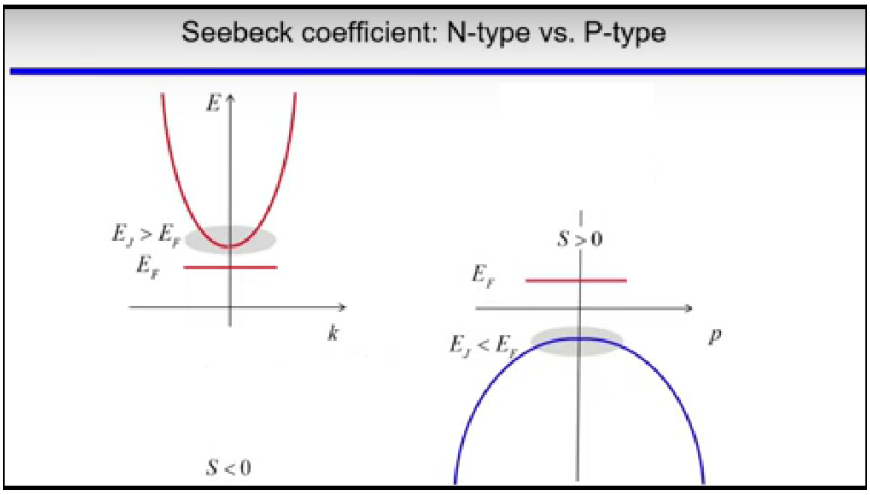

Figure 3.2*: Seebeck coefficient: N-type vs. P-type. The red parabola is the conduction band for an n type semiconductor and the blue parabola is the conduction band for a p type semiconductor. The straight red line in both pictures is the Fermi level. Adapted from [11].*

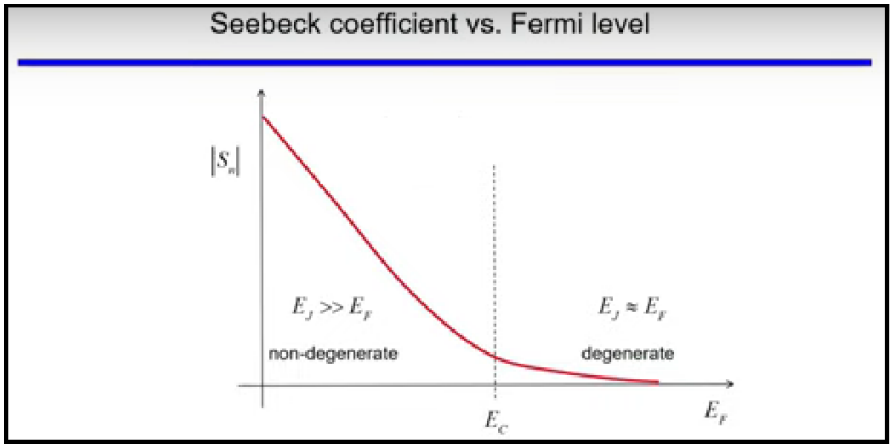

Figure 3.3*: Seebeck coefficient vs Fermi level. The horizontal axis is the Fermi level and the vertical axis is the Seebeck coefficient. The dotted line labeled E_c is the point where the Fermi level is at the edge of the conduction band. Adapted from [11].*

3.3 Thermoelectric Devices [3, 12]

As mentioned previously, the Seebeck and Peltier effects require a junction of two dissimilar materials to occur. Typical thermoelectric devices create these junctions from semiconductors of the same material but different doping types (one n type and the other p type). This will result in the two materials of the junction having individual Seebeck coefficients of equal magnitude but opposite sign, and the Seebeck coefficient of the junction ($\alpha_{AB} = \alpha_A - \alpha_B$) will be twice the individual Seebeck coefficient. In Thermoelectric

generators, many of these junctions are connected in series to combine the individual junction voltages produced by the Seebeck effect.

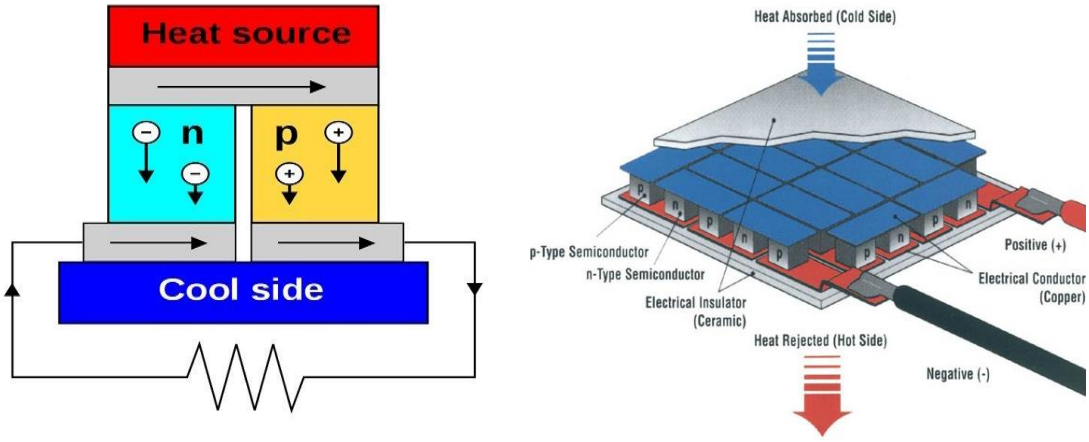

***Figure 3.4**: Thermoelectric device diagrams. The image on the left shows a diagram of an individual p-n junction that would be found in a thermoelectric device. The segments of n type and p type semiconductors are typically referred to as legs. The image on the right shows a diagram of a typical thermoelectric device employing multiple junctions connected electrically in series and thermally in parallel. Adapted from [10,15].*

3.4 Thermoelectric Device Figure of Merit [3, 11, 12]

When calculating the efficiency of devices, a common grouping of the transport coefficients appears and is referred to as the figure of merit. The figure of merit can be made dimensionless by multiplying by temperature.

$$zT = \frac{\alpha^2 \sigma T}{\kappa_L + \kappa_e} \tag{3.9}$$

In the above expression, zT is the dimensionless figure of merit and α is the junction Seebeck coefficient. The efficiency of thermoelectric devices increases when zT is increased. Currently, the highest zT values found in commercially available thermoelectric devices is near 1. It is thought that being able to produce devices with zT values near 3 or 4 could drastically expand the practical applications of thermoelectric devices in industry.

Recent research has suggested that the increase in zT among different materials is parabolically related to the increase in a dimensionless quality factor known as the B factor [11].

$$b = \frac{\sigma}{\kappa_L} T \left(\frac{k_B}{q}\right)^2 \tag{3.10}$$

In the above expression, b is the b factor and k_B is Boltzmann's constant. As can be seen, the only transport coefficients that the b factor depends on are the electrical conductivity coefficient and the lattice thermal conductivity coefficient. If there is no significant deviation from the parabolic relationship between zT and b suggested by research, the only thing that needs to be considered when trying to increase zT is the ratio of electrical conductivity to lattice thermal conductivity. This greatly simplifies the process of searching for and creating better thermoelectric materials as only two transport coefficients need to be engineered rather than several. Recent increases in zT past 1 in research have been greatly attributed to lowering the lattice thermal conductivity while maintaining a greater electrical conductivity.

3.5 Thermoelectric Device Efficiency Limits [3, 12]

One approach to calculating efficiency limits for thermoelectric devices is to apply Dirichlet boundary conditions to a thermoelectric junction. Under these conditions, the hot and cold side are assumed to be at a fixed temperature and thermal contact resistance between the thermoelectric material and the hot and cold sides is ignored. These conditions ignore any change in the temperature between the hot and cold sides due to heat flow across the junction. It is also assumed that the transport coefficients do not change with temperature, which is known as constant property limit (CPL) or constant property model (CPM).

For a single junction thermoelectric generator, the efficiency is found by dividing the output power by the total heat flow through the device and takes into account the joule heating caused by the current and the Peltier effect caused by the current. It is worth noting that during thermoelectric generation, the Peltier effect produced by the current is aligned with the applied temperature difference. In other words, the Peltier heating occurs at the hot side of the device and the Peltier cooling occurs at the cold side. Once the device efficiency is found, it is optimized twice. Once to minimize the heat flow through the device and a second time to maximize the power.

There are two important maximum efficiencies. The first occurs when the load resistance is equal to the total internal resistance of the junction. It is the maximum efficiency when the output power is maximum and is found to be

$$\eta_W = \eta_{Carnot} \frac{0.5}{1+\frac{2}{zT_H}-\frac{\Delta T}{4T_H}} \tag{3.11}$$

In the above expression, η_W is the maximum efficiency at maximum power, η_{Carnot} is the Carnot efficiency $(1-\frac{T_C}{T_H})$, zT_H is the dimensionless figure of merit at the hot side temperature, ΔT is the temperature difference between the hot and cold side, and T_H and T_C are the hot and cold side temperatures respectively.

The overall maximum conversion efficiency occurs when the ratio of the load resistance to the total internal resistance is equal to $\sqrt{1+z\overline{T}}$ where $\overline{T}$ is the average temperature across the device $(\frac{T_H-T_C}{2})$. This efficiency is found to be

$$\eta_{max} = \eta_{Carnot} \frac{\sqrt{1+z\bar{T}}-1}{\sqrt{1+z\bar{T}}+\frac{T_C}{T_H}} \tag{3.12}$$

The max efficiency at maximum power is less than the maximum efficiency overall and the overall maximum efficiency approaches the Carnot efficiency as $z\bar{T}$ approaches infinity.

The Dirichlet boundary conditions hold true when the temperature difference between the hot and cold side is infinitesimal and this property is used in derivations of efficiency limits for different boundary conditions. However, the Dirichlet boundary conditions are not very applicable to real devices and provide a very approximate upper bound to their efficiencies.

A slightly more realistic set of boundary conditions are the Neuman boundary conditions in which the heat flow into and out of the hot and cold sides of the device are considered constant. This approach also assumes CPL and results in max efficiency that coincides with the maximum power output. For any realistic calculation of efficiency limits for real devices, numerical methods are generally employed.

3.6 Thermoelectric Generator Equivalent Circuit [2, 18]

A thermoelectric generator is well modeled by a voltage source (V_{TEG}) in series with a resistance (R_{TEG}). Both are determined by the thermoelectric material characteristics and the temperature difference applied to the generator.

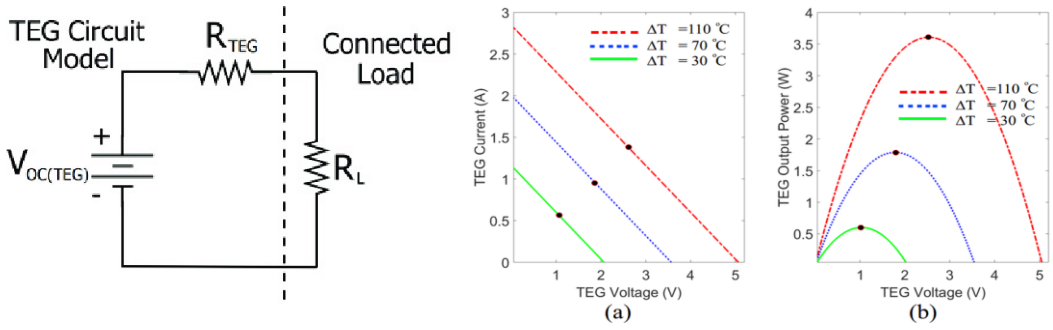

Figure 3.5: *Thermoelectric generator equivalent circuit model. The graphs on the right are examples of the current voltage curve and power curve of the circuit model. Adapted from [5, 24].*

When the load resistance is swept, this circuit produces a straight line for a current voltage curve. The slope of the line is equal to negative one divided by the model resistance and the intercept is equal to the ratio of the model voltage to the model resistance. The maximum power occurs when the load resistance equals the model resistance.

$$m = \frac{-1}{R_{TEG}} \tag{3.13}$$

$$b = \frac{V_{TEG}}{R_{TEG}} \tag{3.14}$$

The voltage at which the max power occurs can be found by taking the power (current times voltage) and setting the first derivative to zero.

$$P = IV = \frac{-1}{R_{TEG}} V^2 + \frac{V_{TEG}}{R_{TEG}} V \tag{3.15}$$

$$\frac{\partial P}{\partial V} = -\frac{2V}{R_{TEG}} + \frac{V_{TEG}}{R_{TEG}} \Rightarrow -\frac{2V_{maxP}}{R_{TEG}} + \frac{V_{TEG}}{R_{TEG}} = 0 \tag{3.16}$$

$$V_{maxP} = \frac{V_{TEG}}{2} \tag{3.17}$$

A similar treatment can be applied to find the current at the max power point.

$$P = IV = -R_{TEG} I^2 + V_{TEG} I \tag{3.18}$$

$$\frac{\partial P}{\partial I} = -2R_{TEG} I + V_{TEG} \Rightarrow = -2R_{TEG} I_{maxP} + V_{TEG} = 0 \tag{3.19}$$

$$I_{maxP} = \frac{V_{TEG}}{2R_{TEG}} \tag{3.20}$$

3.7 Photovoltaic Equivalent Circuit [19]

One common equivalent circuit model of solar cells is the single diode model, which provides a good balance of accuracy and simplicity. The model contains a current source in parallel with an ideal diode. One resistor is in parallel with the diode and a second resistor is in series.

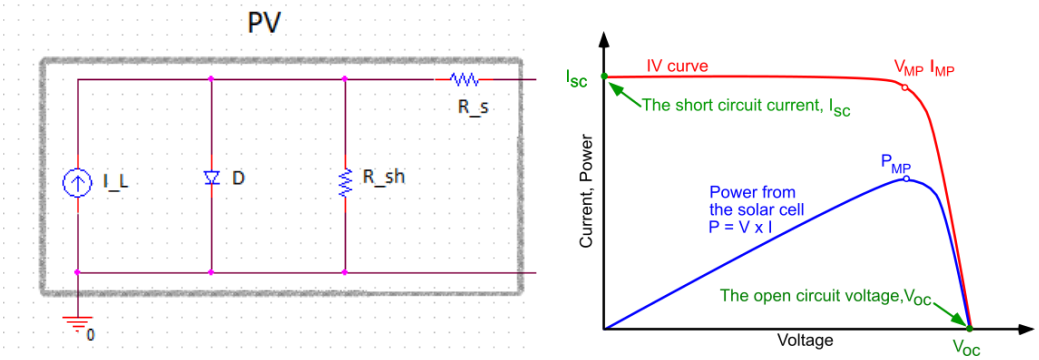

Figure 3.6: *Photovoltaic single diode equivalent circuit model. The graph on the right shows an example of the current voltage curve and power curve of the circuit model. Adapted from [19].*

Using Shockley's equation to model the diode and summing the currents in each branch of the circuit, the equation governing the current voltage relationship of this circuit is found to be the following.

$$I = I_L - I_0\left[e^{\frac{V+IR_S}{nV_T}} - 1\right] - \frac{V+IR_S}{R_{sh}} \tag{3.21}$$

In the above expression, I is the load current, I_L is the current source current, I_0 is the diode saturation current, V is the voltage across the load, n is the diode ideality factor, R_s is the series resistance in the model, R_{sh} is the parallel resistance in the model, and V_T is the thermal voltage which is equal to Boltzmann's constant multiplied by the solar cell temperature and divided by the charge of an electron ($\frac{k_B T}{q}$).

The model equation is found by summing the currents in each branch of the parallel network and using Shockley's equation to model the diode. The model current (I_L) is determined by the irradiance of light on the solar cell and is usually referred to as the photo current. The diode saturation current and resistances are determined by the material properties of the solar cell.

The model equation is a transcendental equation that often appears as a rounded step. Both short circuit (V = 0) and open circuit (I = 0) conditions are also governed by transcendental equations; however, the short circuit current is often very close to the photo current. The max power point occurs at the corner of the step when both the current and voltage are large. The fill factor is the ratio of the max power to the product of open circuit voltage and short circuit current. The smaller the fill factor, the flatter the step is and the smaller the max power.

3.8 Thermoelectric Photovoltaic Series Hybrid Equivalent Circuit [7, 13]

An electrically connected thermoelectric photovoltaic hybrid device can be electrically modeled by connecting the equivalent circuit of a thermoelectric generator to the equivalent circuit of a photovoltaic.

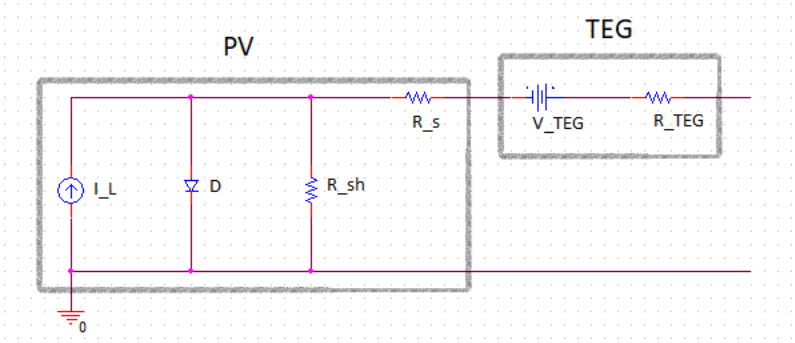

Figure 3.7: *TEG/PV series connected hybrid equivalent circuit model.*

For a series connection, the hybrid circuit model follows the equation below.

$$I = I_L - I_0\left[e^{\frac{V+V_{TEG}+I(R_S+R_{TEG})}{nV_T}} - 1\right] - \frac{V+V_{TEG}+I(R_S+R_{TEG})}{R_{sh}} \tag{3.22}$$

This equation is essentially the same as the photovoltaic single diode model equation, but the thermoelectric generator voltage is added to the open circuit voltage (if attached in the correct orientation) and the thermoelectric generator resistance is added to the series resistance of the photovoltaic element.

Chapter 4: Computer Modeling

Chapter 4 discusses the development of the electrical combination method presented in this work. An equation for modeling the hybrid device is developed from the circuit model and observations about its behavior are presented.

4.1 Starting Point Based on Prior Research

The circuit model of a solar cell in series with a TEG that was presented in [7, 13] was used as the starting point for developing the circuit models in this work.

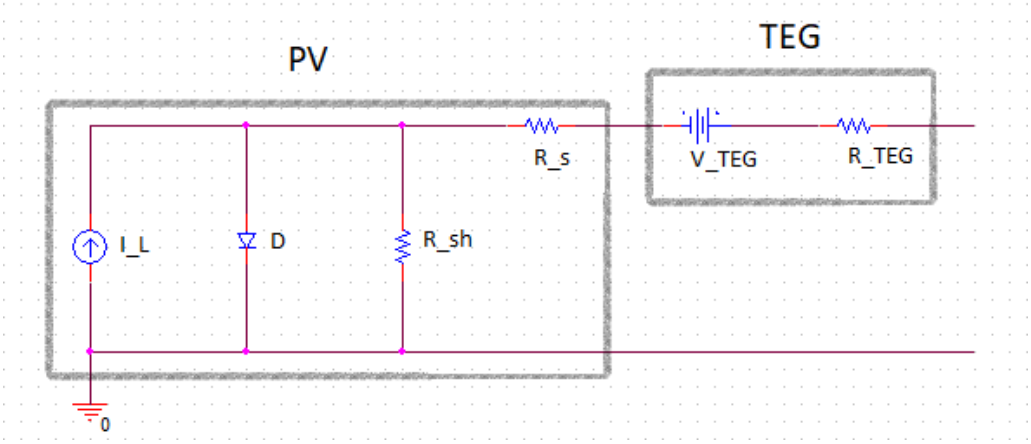

Figure 4.1: *Equivalent circuit model of solar cell in series with a TEG.*

In this model, I_L is the light generated current of the solar cell and D is the diode of the single diode model for the solar cell. It is considered to be an ideal diode following Shockley's equation. It has a reverse saturation current value, a diode ideality factor, and an operating temperature that can be adjusted. R_s and R_{sh} are the series and shunt resistances of the solar cell. V_{TEG} and R_{TEG} are the voltage and resistance of the TEG. The model parameters just described can all be adjusted and their values correspond to operating conditions such as light level and temperature, as well as physical characteristics of the materials used in the device.

4.2 Unsuccessful Method of Electrically Combining PV and TEG

Before investigating the parallel network method for combining the power of the TEG and PV element, another related method was tested. In this method, a resistor is added in parallel to the TEG.

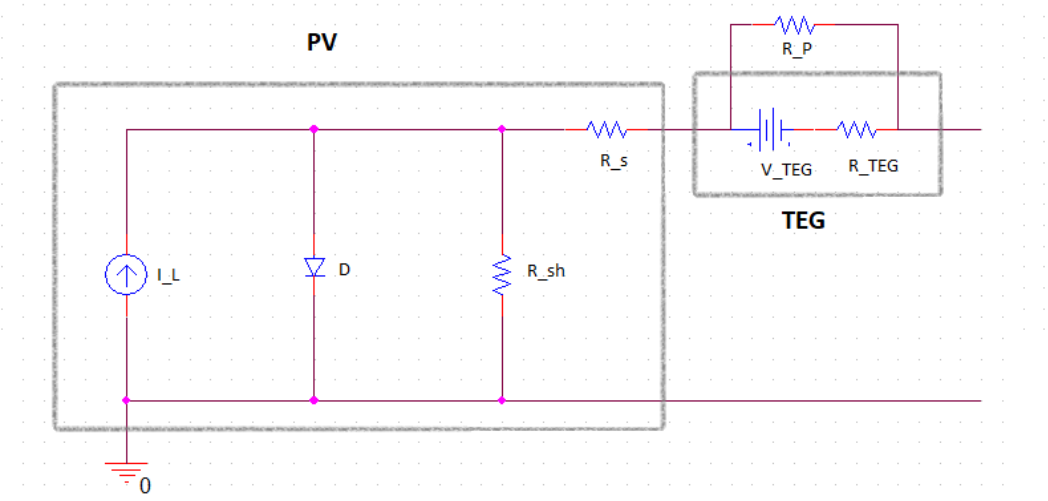

Figure 4.2: *Circuit model of parallel resistor method to combine TEG and PV element power.*

The thinking behind this is that the series resistance of the TEG and the added resistor will have a lower equivalent resistance since they are in parallel. This lowers the value of resistance in series with the PV element which should improve the fill factor of the hybrid device. Thinking about the extreme cases of this circuit, if the parallel resistor has infinite resistance, it is as if the resistor is not there and the circuit is equivalent to the unmodified PV/TEG series hybrid device. If the parallel resistor is zero, it acts as a short circuit bypassing the TEG and making the whole device equivalent to just the PV element. Perhaps there is some value for the parallel resistor that lies between these two cases and results in the hybrid device having a max power that is some combination of the TEG and PV element max powers.

PSPICE was used to simulate this circuit model to investigate its viability in combining the TEG and PV element powers. It was found that no addition of the two powers is possible with this method. As expected, for high values of the parallel resistor the circuit behaved like the unmodified PV/TEG series hybrid device. As the parallel resistor value was decreased, the fill factor of the hybrid device did improve. However, the hybrid device's max power was never greater than the max power of the PV element alone and merely approached this value as the value of the parallel resistor was decreased towards zero. This behavior was observed for several different sets of model parameter values and seems to be general.

4.3 Parallel TEG Network Method for Electrically Combining PV and TEG

The second method for combining the TEG and PV element power that was investigated was the parallel TEG network method. In this approach, the TEG itself is divided into a parallel network of sub-TEGs. This is possible because the original TEG consists of a number of pairs of legs all connected in series to achieve the greatest voltage.

When divided into N sub-TEGs, each sub-TEG will have a voltage of the original TEG's voltage (V_{TEG}) divided by N and a resistance of the original TEG's resistance (R_{TEG}) divided by N. This is valid if the

temperature conditions applied to the original TEG are unchanged and only the electrical connections of the leg pairs in the TEG are altered. It also assumes that each pair of legs in the original TEG can be considered identical.

The first benefit of this method is the reduction in series resistance added by the TEG. This resistance is reduced directly from the splitting in addition to the reduction due to the sub-TEG resistances being in parallel.

The second benefit is the PV element current being divided into each of the sub-TEGs. In chapter 3 it was shown that for a TEG, the voltage at which the max power occurs is ½ the TEG voltage and that the current at which the max power occurs was ½ the ratio of the TEG voltage to the TEG resistance. From this it can be seen that at the max power point the splitting of the TEG will reduce the voltage of the sub-TEGs. However, since the max power point current depends on the ratio of the TEG voltage to TEG resistance, the current of each sub-TEG will be the same as the original unsplit TEG. This combined with the dividing of the PV element's current leads to less mismatch between the two currents.

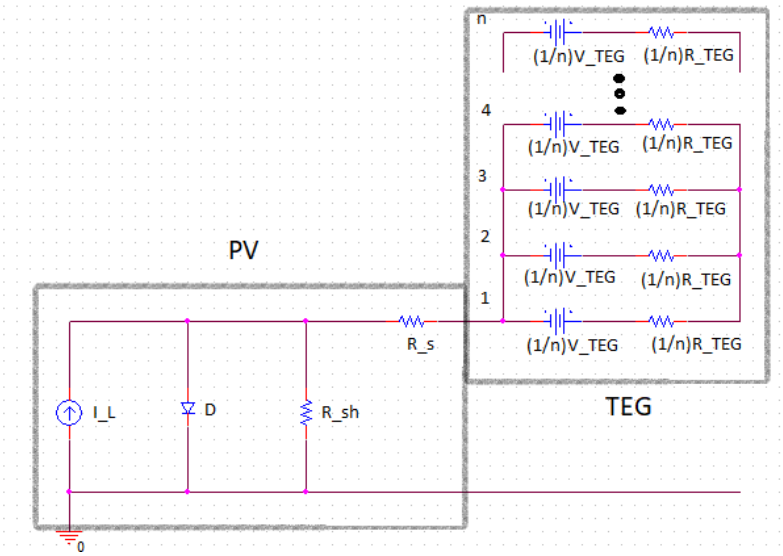

Figure 4.3: *Circuit model of PV/TEG series hybrid device with parallel TEG network for splitting level n.*

I will refer to N as the splitting level of the TEG parallel network. For example, if the original TEG is divided into 3 sub-TEGs, then the splitting level is 3 and each sub-TEG will have a voltage of 1/3 V_{TEG} and a resistance of 1/3 R_{TEG}. It should also be noted that the number of achievable splits is limited by the number of leg pairs in the original TEG, i.e., a TEG with M pairs of legs can be split a maximum of M times.

4.4 Linear Approximation of TEG Parallel Network

In order to produce an equation for the current voltage behavior of this circuit model, the TEG parallel network needs to be simplified. This was done by applying the linear methods of superposition and Thevenin's equivalent circuit to the TEG parallel network. This is an approximation since these methods apply to linear circuits only and the total circuit model is non-linear due to the presence of the diode.

The parallel network of TEGs is the linear network to be converted into a Thevenin voltage and resistance while the rest of the circuit is considered the load. First, the Thevenin voltage is found by disconnecting the load and finding the voltage across the remaining circuit.

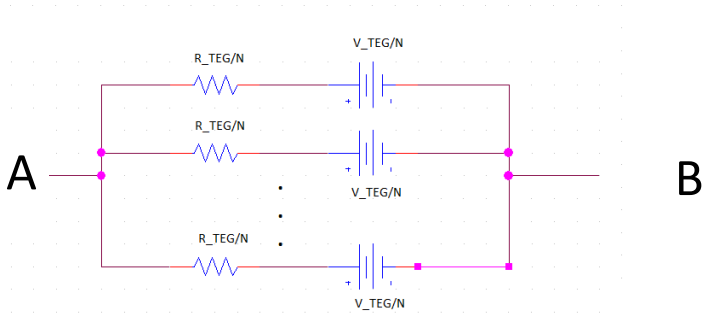

Figure 4.4: *TEG parallel network with the remaining circuit, or load, disconnected.*

To deal with the multiple voltage sources, superposition will be applied. This is done by shorting all the voltage sources in the circuit but one for each of the individual voltage sources. The total voltage between points A and B is the sum of the voltages between points A and B for each of these cases.

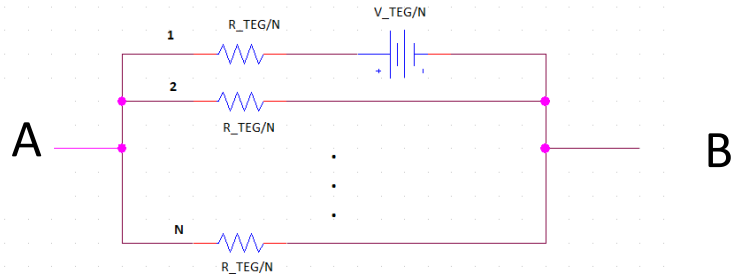

Figure 4.5: *One case of shorting each voltage source but one for the first voltage source in the sequence.*

There are N-1 resistors in parallel without a voltage source next to them. These can be combined into the following equivalent resistance due to their parallel connection.

$$R_{eq} = \frac{R_{TEG}}{N}\frac{1}{(N-1)} \tag{4.1}$$

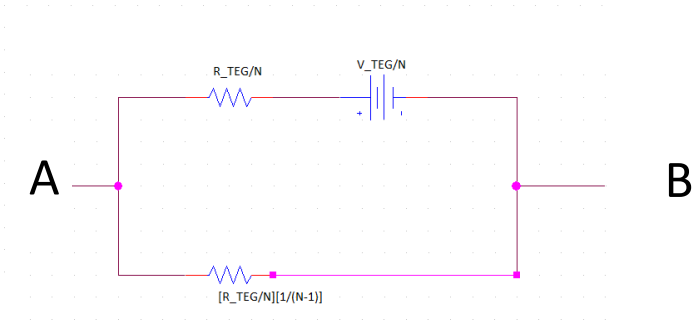

Figure 4.6: *Circuit from Figure 15 with equivalent resistance applied.*

The circuit in Figure 4.6 forms a loop and the current in the loop can be found by dividing the voltage source by the total resistance, which is just Ohm's Law.

$$i = \frac{\frac{V_{TEG}}{N}}{\frac{R_{TEG}}{N}+\frac{R_{TEG}}{N}\frac{1}{(N-1)}} = \frac{\frac{V_{TEG}}{N}}{\frac{NR_{TEG}}{N(N-1)}} = \frac{V_{TEG}(N-1)}{NR_{TEG}} \tag{4.2}$$

The voltage drop across the first resistor is found by multiplying the current by the resistor value, which is also just Ohm's Law.

$$V_{drop} = i\frac{R_{TEG}}{N} = \frac{V_{TEG}(N-1)}{NR_{TEG}}\frac{R_{TEG}}{N} = \frac{V_{TEG}(N-1)}{N^2} \tag{4.3}$$

The voltage between points A and B is just this voltage drop subtracted from the voltage source.

$$V_{AB} = \frac{V_{TEG}}{N} - V_{drop} = \frac{V_{TEG}}{N} - \frac{V_{TEG}(N-1)}{N^2} = \frac{V_{TEG}}{N^2} \tag{4.4}$$

All of the other cases of shorting every voltage source but one are identical to this case. This means that the sum of all these voltages is just N multiplied by the result of the first case above.

$$V_{th} = V_{ABtotal} = N\frac{V_{TEG}}{N^2} = \frac{V_{TEG}}{N} \tag{4.5}$$

Now that the Thevenin voltage is found, the Thevenin resistance is all that remains. This is found by shorting all of the voltage sources and finding the equivalent resistance between points A and B.

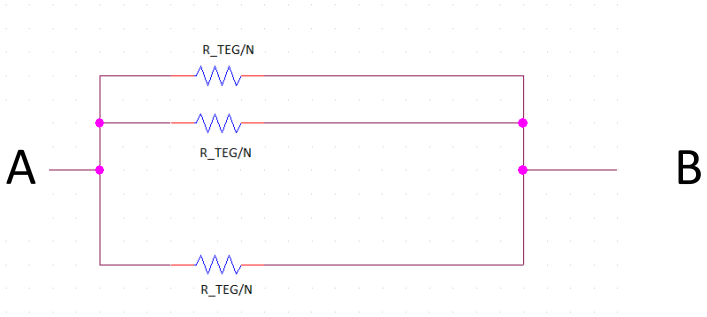

Figure 4.7: *Circuit from Figure 14 with all of the voltage sources shorted.*

The total resistance between points A and B is simply found by combining the N parallel resistors into their equivalent resistance.

$$\frac{1}{R_{th}} = \frac{N}{\frac{R_{TEG}}{N}} \Rightarrow R_{th} = \frac{R_{TEG}}{N^2} \tag{4.6}$$

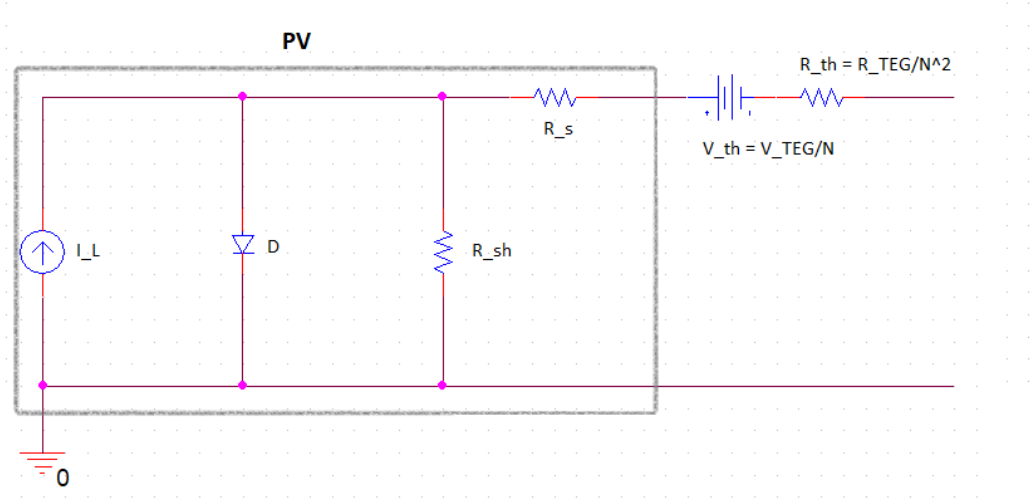

Figure 4.8: *Thevenin equivalent of the circuit in Figure 13 using the linear approximation.*

As can be seen, the Thevenin equivalent circuit is has the same form as the circuit model from the starting point but with slight modification to the values of the TEG voltage and resistor. The same current analysis that was used in the prior research can be applied to get the following equation for the current voltage behavior of this circuit model. All of the variables are the same as in Equation 2.1 and it should be noted that n is still the diode ideality factor and N is the splitting level applied to the TEG.

$$I = I_L - I_0\left[e^{\frac{V+\frac{V_{TEG}}{N}+I(R_S+\frac{R_{TEG}}{N^2})}{nV_T}} - 1\right] - \frac{V+\frac{V_{TEG}}{N}+I(R_S+\frac{R_{TEG}}{N^2})}{R_{sh}} \tag{4.7}$$

4.5 Matlab Model

Equation 4.7 is a transcendental equation and can only be modeled using numerical methods. To do this, Matlab was used. The fzero function was used to find solutions to Equation 4.7 with respect to the variable I. V was treated as some constant like all of the model parameters. The fzero function starts with some initial guess for solving the equation f(x) = 0. Through an iterative process, the guess is improved to an accurate approximation of the actual value. A for loop repeated this process for many values of V to generate a collection of IV points. This is how the IV curves of this model were produced. A copy of the code for this model is shown below.

```
%% PV/TEG Series Hybrid with Parallel TEG Network Model
% User defined input parameters of circuit model
Vteg_initial=7; %% Initial TEG Voltage
Rteg_initial=10; %% Initial TEG Resistance
N=10; %% Splitting Level of TEG
Vteg=(1/N)*Vteg_initial; %%Equivalent TEG Voltage in Volts After N Division
Rteg=((1/N).^2)*Rteg_initial; %%Equivalent TEG Series Resistance in Ohms After N Division
Rs=0.01; %%Solar Cell Series Resistance in Ohms
R=Rteg+Rs;
Rsh=10000; %%Solar Cell Shunt Resistance
T=300.15; %%Temperature of Diode
Io=10.^(-11); %%Reverse Saturation Current of Diode
IL=4; %%Light Generated Current
Vt=(8.6173*(10.^(-5)))*T; %%Thermal Voltage (Boltzmann and Charge Constants Combined)
n=1; %Diode Ideality Factor

Vstart=0; %Initial voltage
Vstop=0.75; %Final voltage
stp=1000; %Number of points in simulation
Vinc=(Vstop-Vstart)/stp;
Vfinal=zeros(stp,1);
Ifinal=zeros(stp,1);

for i=1:stp
   V=(i-1).*Vinc; %  V value of current iteration
   % f(x) to be solved by fzero
   f=@(x,V,Vteg,R,Io,IL,Vt,Rsh,n)x+(Io*(exp((V-Vteg+(x*R))/(n.*Vt))-1))+((V-Vteg+(x*R))/Rsh)-IL;
   x0=0; % initial guess for fzero
   r=fzero(@(x)f(x,V,Vteg,R,Io,IL,Vt,Rsh,n),x0);
   Vfinal(i)=V; % V values of IV curve
   Ifinal(i)=r; % I values of IV curve
end

Pwr=Vfinal.*Ifinal; %power values
```

4.6 Results of Modeling

The first thing that was done was to compare the PSPICE model, which does not use the linearity approximation, to the Matlab model, which does use this approximation. It was found that the two models are nearly identical. An example of this is shown below.

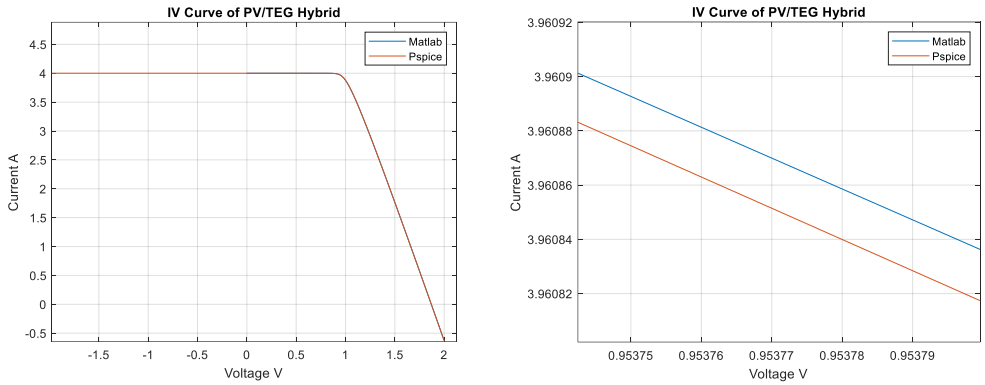

Figure 4.9: *Comparison of PSPICE and Matlab models for same model parameters and splitting level. The graph on the right is an enlarged version of the graph on the left.*

As can be seen in Figure 4.9, the difference between the two models is miniscule. This was repeated for numerous sets of model parameters and splitting levels. The difference between the two models was always less than 0.001% of the non-approximate (PSPICE) value. This provides empirical support for the linear approximation used to make the Matlab model. Since the Matlab model is easier to work with, this model was used for the remaining investigation of the circuit model.

The primary result of the computer modeling was that the PV element power and TEG power are able to achieve lossless electrical combination with the parallel network method. The figure below shows an example of this behavior.

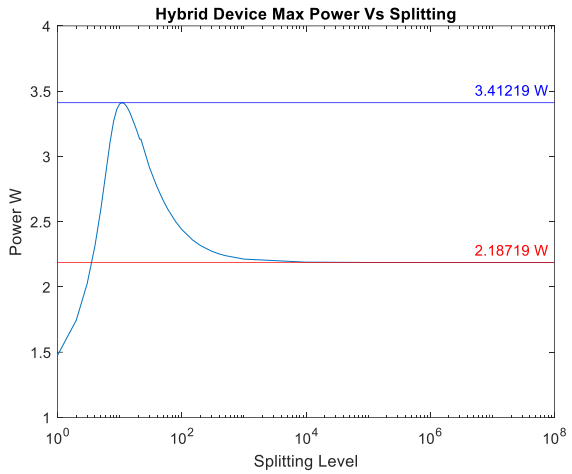

Figure 4.10: *PV/TEG series hybrid with parallel TEG network max power versus splitting level. The red horizontal line is the max power of the PV element by itself and the blue horizontal line is the sum of the PV element max power with the TEG max power. The splitting level is on a logarithmic scale.*

In Figure 4.10, it can be seen that the hybrid device starts at a max power that is lower than the PV elements initial max power. As the splitting level increases, the hybrid device's max power gradually improves. At a splitting level of 11, the hybrid device's max power is a nearly perfect sum (between 99% and 100%) of the PV element max power and TEG max power. As the splitting level is further increased, the hybrid device's max power decreases and seems to approach the PV element's max power as the splitting level approaches infinity. Note the use of the logarithmic scale and how much slower the decrease in max power after the optimal splitting level is compared to the increase in max power before the optimal splitting level.

The plot in Figure 4.10 was for a specific set of circuit model parameter values, but the model was run for a number of different sets of parameters and this behavior was observed for each one. Empirically, the behavior appears to be a general property of the circuit model.

An additional interesting feature of the model that was noticed is that the effect of the TEG on the fill factor is related to how much of a power contribution the TEG is making. If the TEG max power is very small compared to the PV element's power, adding the TEG in series has little to no effect on the fill factor and the hybrid device's IV curve resembles the PV element IV curve. If the TEG max power is a significant percent of the PV element's max power, adding the TEG in series has a much more noticeable effect and the hybrid device's IV curve will have a very degraded fill factor.

Chapter 5: Experimental Work

Chapter 5 presents the experimental setup for a thermoelectric/photovoltaic hybrid device that was used in this work. Data collection and statistical treatment are also discussed. The data collected from this setup is presented, along with predictions made by the model developed in chapter 4. A summary of observations based on the data is also included.

5.1 Experimental Setup

To make a PV/TEG series connected hybrid device, commercial solar cell and TEG modules were used. The solar cell modules used were the Sunyima 50x50 millimeter polycrystalline modules. The TEGs used were the Hilitand 40x40 millimeter thermoelectric Peltier modules. These modules use bismuth telluride for the thermoelectric material and are intended for cooling, but will still produce thermoelectric generation. Each TEG module had a solar cell module connected to it with thermally conductive double-sided tape. Wires that could be connected into a breadboard were soldered to the positive and negative terminals of each individual solar cell module and TEG module. This way, the all the electrical connections are through the breadboard and can be changed whenever desired.

The light source used to power the hybrid device was a Verilux 12499 full spectrum light bulb. The light from the bulb powers the solar module part of the device, which leads to the production of waste heat. The TEG module attached to the solar module has one side heated by the waste heat and the other side cooled by the ambient air. This produces a temperature gradient across the TEG module that leads to a voltage difference being produced. A potentiometer was connected as a variable resistor load to the device through the breadboard. A Fluke 87-V and a Fluke 101 multimeter were used to take current and voltage measurements to produce IV curves.

Six of the TEG modules in series were used as the initial unsplit TEG. By adding parallel connections, splitting levels of 2, 3, and 6 could be achieved. For example, making 3 groups of 2 modules in series and connecting those 3 groups in parallel achieves a splitting level of 3. Each module had a solar cell module attached with the thermal tape. The solar cell modules could be attached in series, parallel, or some combination of the two to act as a larger solar cell. Some solar cell modules could also be excluded from the electrical connection altogether. It only affects the model parameters of the PV element part of the hybrid device’s circuit model.

Figure 5.1*: Thermoelectric Modules used in experimental setup.*

Four different runs with different modifications made to the device were executed. In the first run, the six solar cell modules were connected in series to act as the PV element. The PV/TEG modules were arranged in a grid pattern that was 2x3 modules in area. The device was allowed to sit beneath the light for 20 minutes before taking measurements to allow for the operating temperatures to stabilize. IV curve measurements were taken for the PV element by itself, the unsplit TEG by itself, and the hybrid device for split levels of 1, 2, 3, and 6. Each sub-TEG for each of the split levels also had IV measurements taken. When measuring the PV element or TEG components by themselves, the solar cell modules were kept thermally attached to the TEG modules with the tape. Also, the surface temperature of the solar cell module in each TEG/PV module was measured with the Fluke 87-V multimeter. The distance between the light and device was not measured for this run.

Figure 5.2*: Grid pattern of PV/TEG modules used in Run 1.*

For the second run, everything was kept the same as with the first run except the PV/TEG modules were arranged in a circular pattern beneath the light bulb. This was to try and make the light/temperature conditions on each TEG/PV module as identical as possible since the circuit model assumes that the TEGs are being split evenly. The same measurement process as in the first run was used here. The distance between the light and device was about 30 cm.

Figure 5.3: *Circular pattern of PV/TEG modules used in Runs 2, 3, and 4.*

For the third run, everything was kept the same as the second run except only three of the solar cell modules in series were used as the PV element of the hybrid device. This was to make the power contribution of the TEG element more significant. The other three solar cell modules remained attached to the TEG modules with the thermal tape but were not electrically connected. The same measurement process as in the first and second runs was used here. The distance between the light and the device was about 7 cm.

For the fourth run, everything was kept the same as the third run except only one of the solar cell modules was used as the PV element of the hybrid device. This was to further increase the significance of the TEG element's power contribution. The other five solar cell modules remained attached to the TEG modules with the thermal tape but were not electrically connected. The same measurement process as in the previous runs was used here. The distance between the light and the device was about 14 cm.

5.2 Model Parameter Extraction

For each run, the model parameters for the PV element and unsplit TEG must be extracted from the measured data of the PV element by itself and the TEG by itself. The single diode model for the PV element produces a relatively complicated IV curve that does not lend itself well to calculation based fitting methods. Because of this, the parameter values were matched to the PV element data points by visual inspections. In other words, the model parameters were tweaked until it produced an IV curve that visually matched the data points as close as possible. Since the TEG IV curve is a straight line, a least squares fit was used to match the data points to their line of best fit. From this line, the TEG voltage and resistance could be calculated.

5.3 Fit Analysis

To statistically analyze the data and determine if it fits the models well, a method based on the residual standard error (RSE) was used. The residual standard error is calculated with the following formula.

$$RSE = \sum_{a=1}^{A} \frac{\sqrt{(measured\ value_a - expected\ value_a)^2}}{number\ of\ degrees\ of\ freedom} \quad (5.1)$$

The residual standard error measures the average difference between the data points and the model predictions in units of the measured value. In this experiment, the measured values are the current measurements that are being matched to voltage measurements. The higher the RSE, the worse the data is fitted to the model.

In order to determine whether or not the fit is good, I will compare the RSE to the expected experimental error (EEE). If the ratio of the RSE to the EEE is 1 or less, all the difference between the data points and model predictions can be accounted for by the EEE. This is what I will consider a good fit. If the ratio of the RSE to the EEE is greater than 1, then the difference between the data points and model predictions is not well accounted for by the EEE. This will not be considered a good fit.

Also, two of my data points (the short circuit current and open circuit voltage) directly determine parameter values in the model and thus will not contribute any error. These points are not considered degrees of freedom and do not get counted in the number of degrees of freedom. Thus, my number of degrees of freedom for each data set will be the number of data points minus 2.

5.4 Measurement Error

The experimental setup has a number of error sources. Firstly, the multimeters have a listed measurement error of less than 0.1%. There is also error due to the fluctuation of light and temperature conditions that occurs over the time it takes to collect all of the IV measurements for a given device. Since the IV measurements are being taken manually, some time passes from the first to last measurement taken. In that time, the light and temperature conditions on the measured device can change due to a number of reasons such as changes in the room temperature or changes in the light being emitted by the bulb.

To estimate the measurement error, the IV measurements of the PV element by itself were used. The single diode model of the PV element was assumed to be accurate and provide a good fit. This means that whatever discrepancy was between the data points and the fitted model parameters was due to experimental error. The value of the experimental error was found by selecting an error value that made the ratio of the RSE and EEE equal to 1. The power of each data point is found by multiplying the voltage by the current. Thus, the error in each power measurement is the current error multiplied by the voltage.

5.5 Run 1 Data

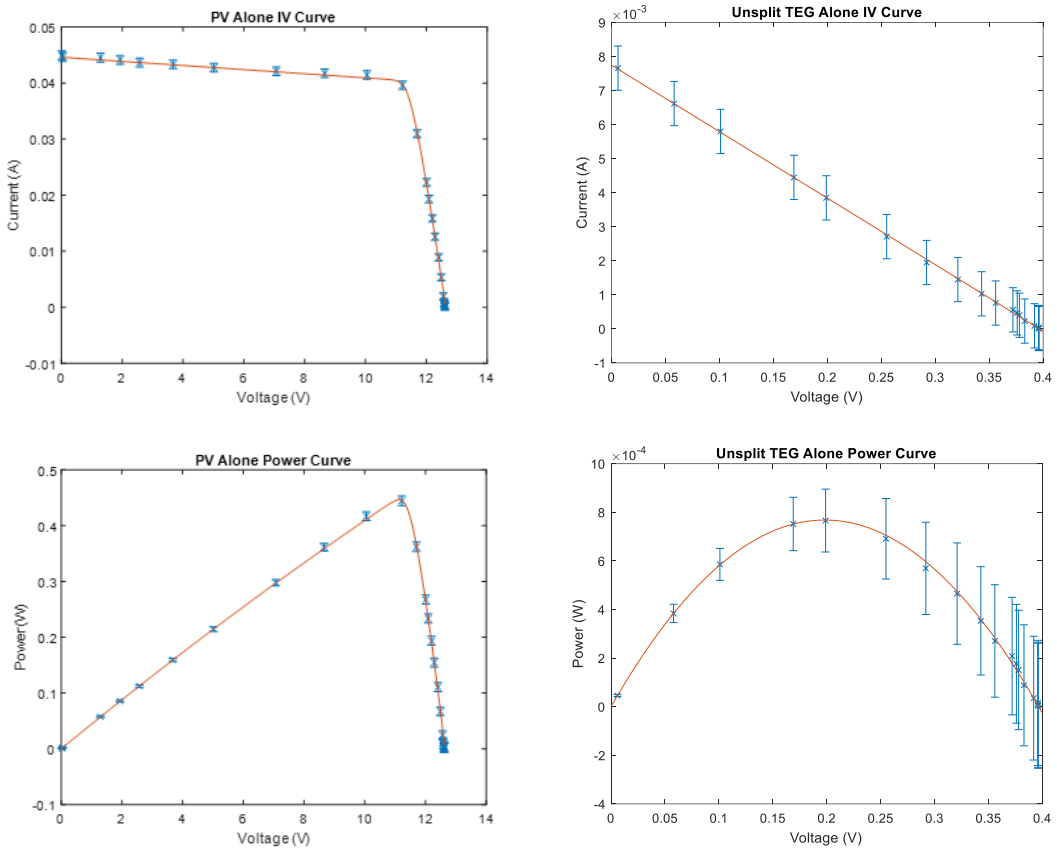

Figure 5.4: *Run 1 IV and power data points for PV element alone and unsplit TEG alone. The experimental error in the current was estimated to be 0.00062 A using the method described above. The error in the power data points is the voltage multiplied by the current error. The solid line curve in the PV element plot is the single diode model for parameters that best fit the data points. The solid line in the TEG plot is the least squares fit line for the data points. The number of data points in the PV IV plot is 25 and the RSE/EEE ratio using the error of 0.00062 A is 0.998. The measured max power of the TEG is 0.000768 W and the measured max power of the PV element is 0.445 W.*

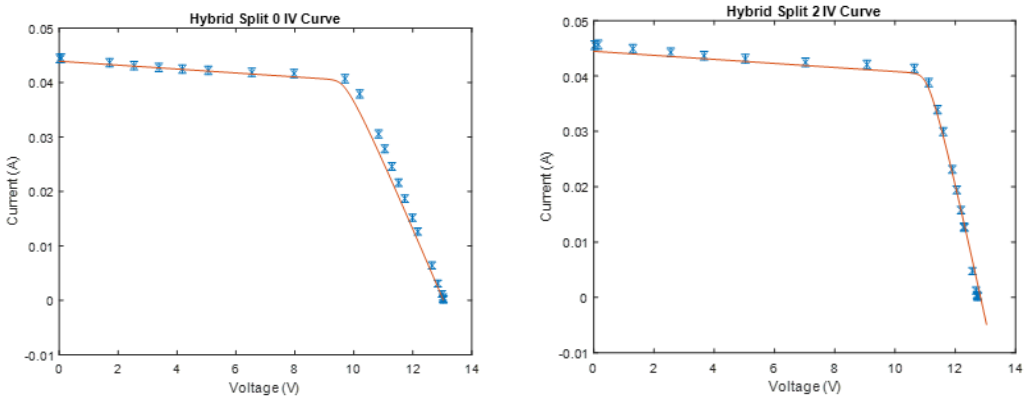

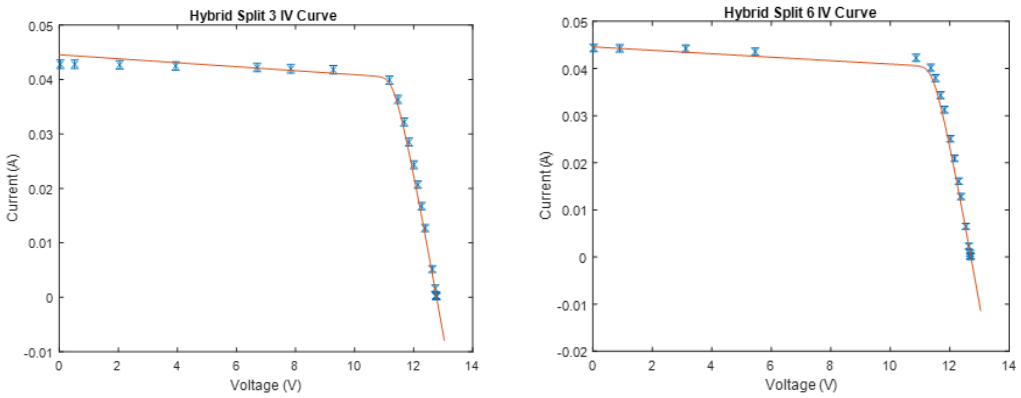

Figure 5.5: *Run 1 data points for PV/TEG series hybrid with no splitting, splitting level 2, splitting level 3, and splitting level 6. The current experimental error is 0.00062 A as previously stated. The solid lines are the expected current values predicted by the circuit model. The RSE/EEE ratios are 7.54, 5.02, 4.62, and 7.18 respectively. The number of data points in each plot are 25, 23, 20, and 19 respectively.*

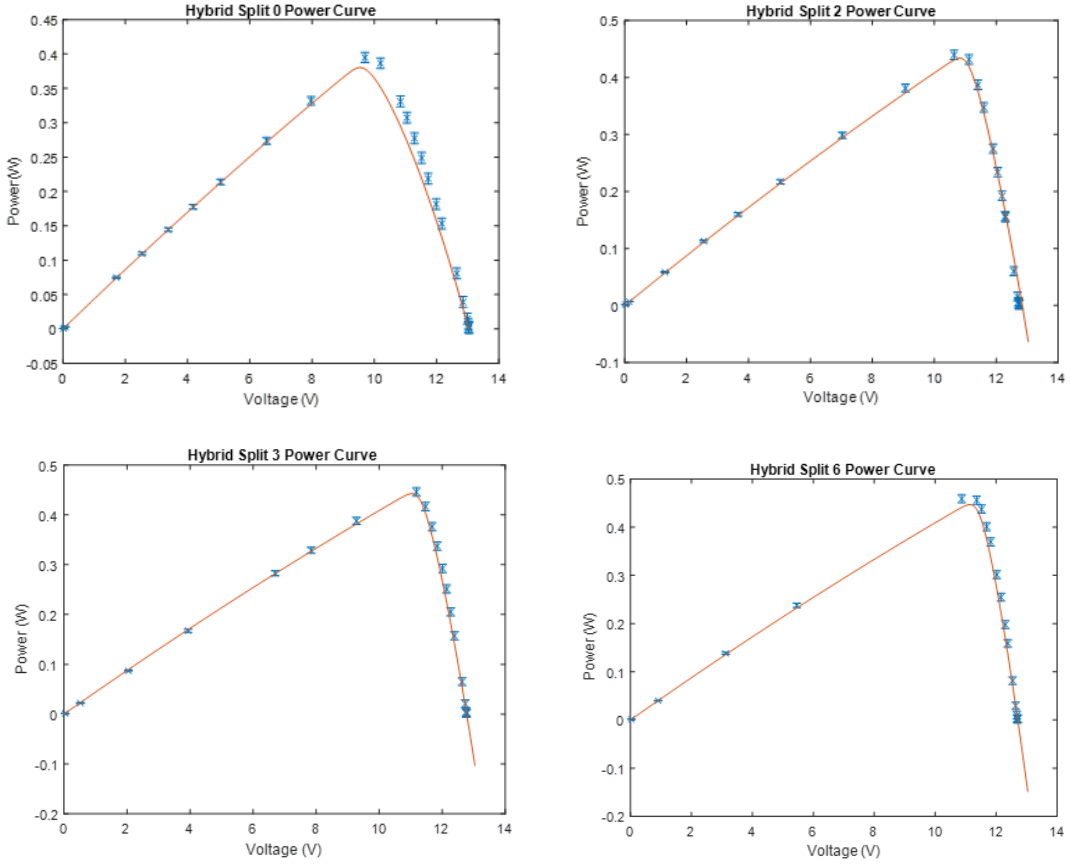

Figure 5.6: *Run 1 power curves for PV/TEG series hybrid with no splitting, splitting level 2, splitting level 3, and splitting level 6. The error of each point is the current error (0.00065 A) multiplied by the voltage. The solid lines are the power curves predicted by the circuit model. The lowest power measurement error is 0.000011 W and the largest is 0.0085 W.*

	(1,2,3,4,5,6)	*(1,2,3)*	*(4,5,6)*	*(1,2)*	*(3,4)*	*(5,6)*
Voltage	0.3949 V	0.1562 V	0.2366 V	0.085 V	0.1716 V	0.1323 V
Resistance	51.28 Ω	20.28 Ω	31.55 Ω	15.75 Ω	12.804 Ω	26.46 Ω

	(1)	*(2)*	*(3)*	*(4)*	*(5)*	*(6)*
Voltage	0.0384 V	0.048 V	0.0696 V	0.0987 V	0.0727 V	0.0549 V
Resistance	6.627 Ω	9.794 Ω	7.734 Ω	6.901 Ω	22.03 Ω	6.693 Ω
Temperature	45.6 °C	43.9 °C	-	-	-	-

Table 5.1: *Run 1 sub-TEG voltage and resistance values. (1,2,3,4,5,6) corresponds to the unsplit TEG, (1,2,3) and (4,5,6) correspond to the sub-TEGs for the splitting level of 2, and so forth. The surface temperatures of each TEG/PV module are also listed. The temperature measurements for TEGs 3, 4, 5, and 6 were lost.*

5.6 Run 2 Data

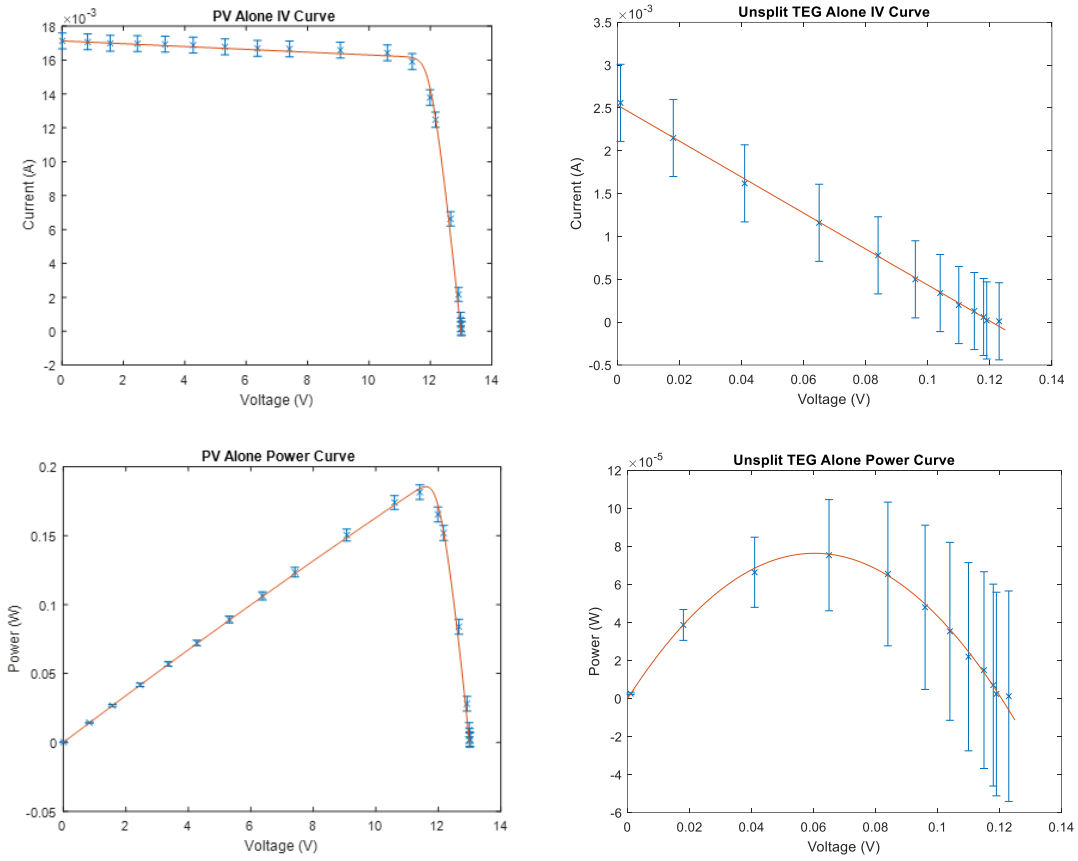

Figure 5.7: *Run 2 IV and power data points for PV element alone and unsplit TEG alone. The experimental error in the current was estimated to be 0.00042 A using the method described above. The error in the power data points is the voltage multiplied by the current error. The solid line curve in the PV element plot is the single diode model for parameters that best fit the data points. The solid line in the TEG plot is the least squares fit line for the data points. The number of data points in the PV IV plot is 20 and the RSE/EEE ratio using the error of 0.00042 A is 1.00. The measured max power of the TEG is 0.0000758 W and the measured max power of the PV element is 0.181 W.*

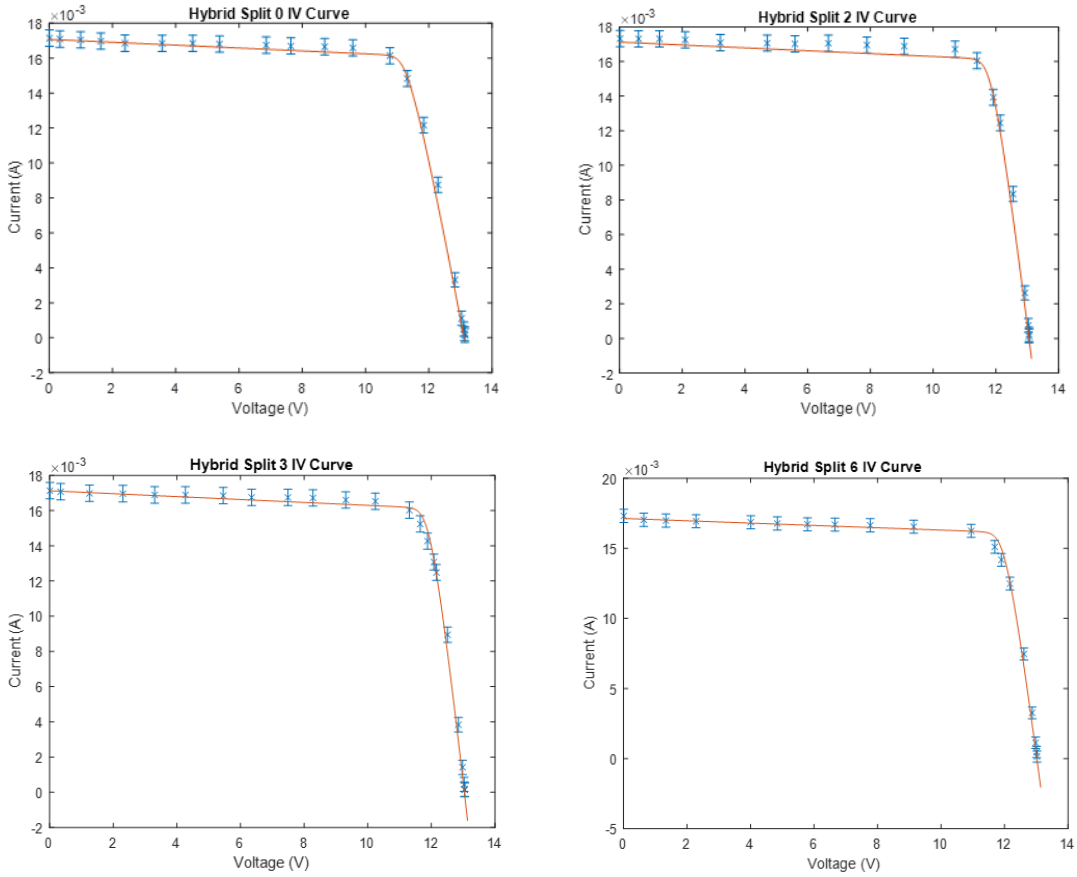

Figure 5.8: *Run 2 data points for PV/TEG series hybrid with no splitting, splitting level 2, splitting level 3, and splitting level 6. The current experimental error is 0.00042 A as previously stated. The solid lines are the expected current values predicted by the circuit model. The RSE/EEE ratios are 0.993, 1.630, 0.955, and 1.090 respectively. The number of data points in each plot are 21, 19, 23, and 19 respectively.*

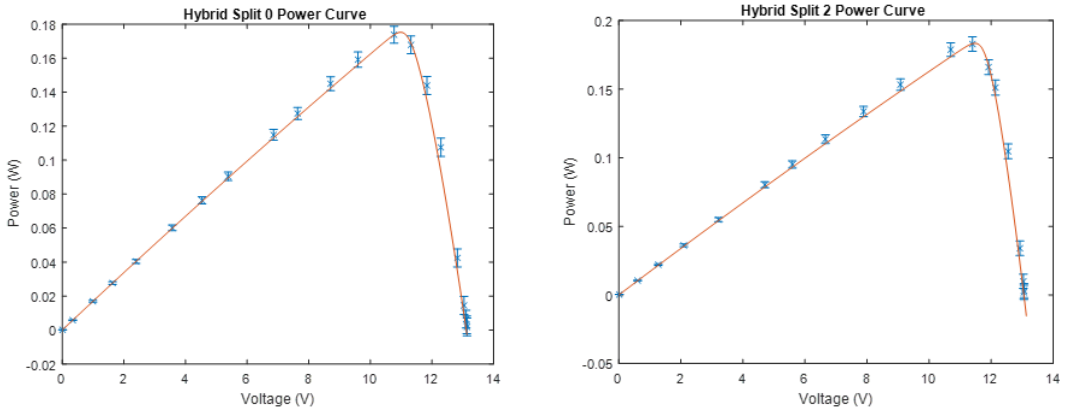

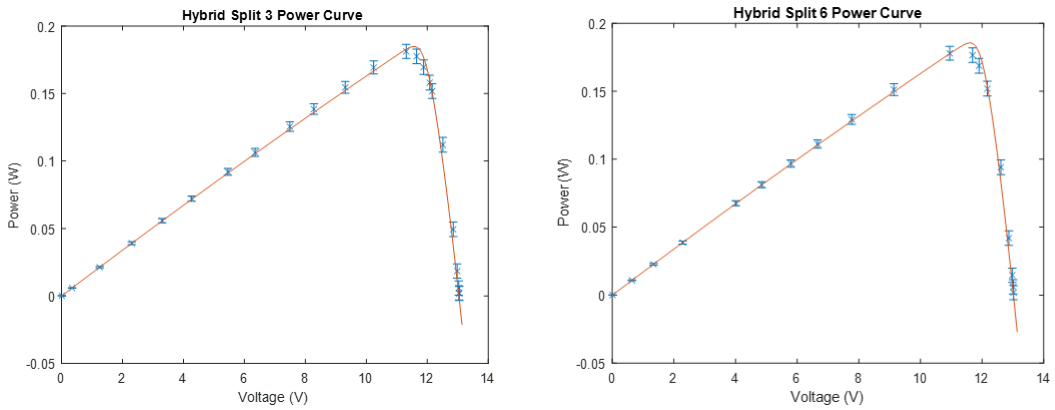

Figure 5.9: *Run 2 power curves for PV/TEG series hybrid with no splitting, splitting level 2, splitting level 3, and splitting level 6. The error of each point is the current error (0.00042 A) multiplied by the voltage. The solid lines are the power curves predicted by the circuit model. The lowest power measurement error is 0.00000422 W and the largest is 0.0055 W.*

	(1,2,3,4,5,6)	*(1,2,3)*	*(4,5,6)*	*(1,2)*	*(3,4)*	*(5,6)*
Voltage	0.119 V	0.0502 V	0.0886 V	0.0282 V	0.05 V	0.0591 V
Resistance	47.62 Ω	18.59 Ω	28.57 Ω	14.08 Ω	10 Ω	24.63 Ω

	(1)	*(2)*	*(3)*	*(4)*	*(5)*	*(6)*
Voltage	0.0129 V	0.0137 V	0.0195 V	0.0314 V	0.0393 V	0.0181 V
Resistance	6.45 Ω	10.54 Ω	7.23 Ω	6.676 Ω	19.65 Ω	6.96 Ω
Temperature	29.3 °C	30.4 °C	32.7 °C	37.4 °C	37.0 °C	31.6 °C

Table 5.2: *Run 2 sub-TEG voltage and resistance values. (1,2,3,4,5,6) corresponds to the unsplit TEG, (1,2,3) and (4,5,6) correspond to the sub-TEGs for the splitting level of 2, and so forth. The surface temperatures of each TEG/PV module are also listed.*

5.7 Run 3 Data

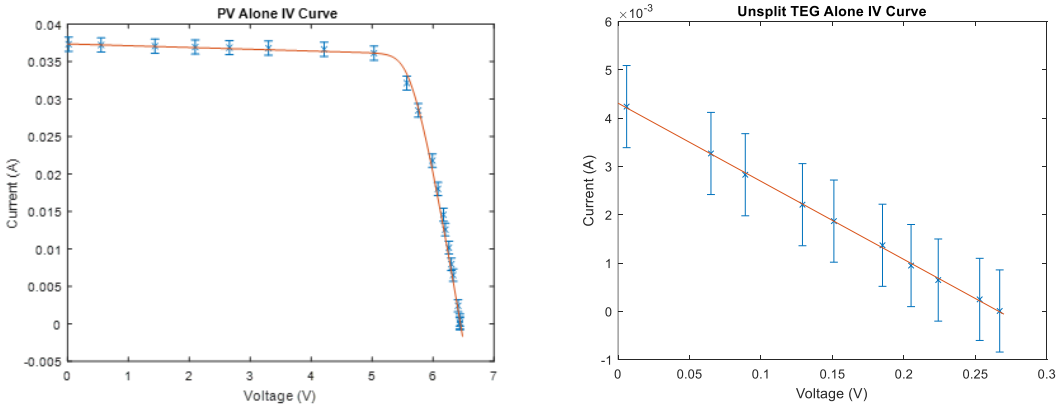

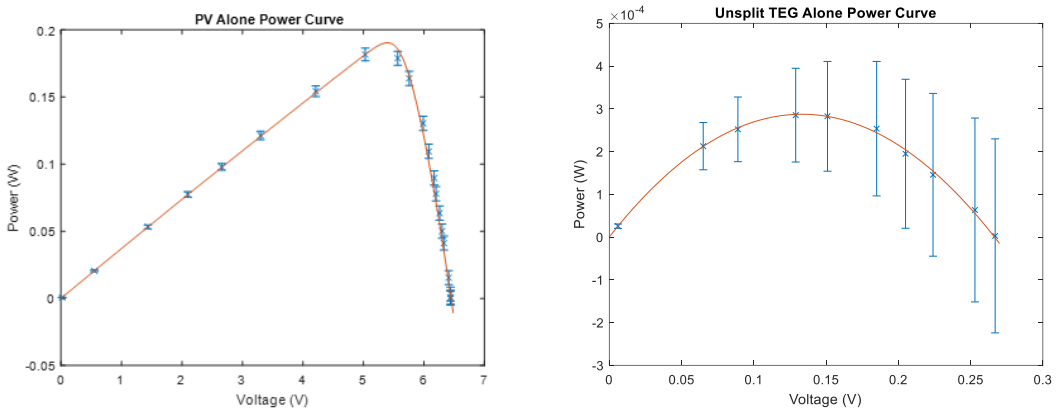

Figure 5.10: *Run 3 IV and power data points for PV element alone and unsplit TEG alone. The experimental error in the current was estimated to be 0.00085 A using the method described above. The error in the power data points is the voltage multiplied by the current error. The solid line curve in the PV element plot is the single diode model for parameters that best fit the data points. The solid line in the TEG plot is the least squares fit line for the data points. The number of data points in the PV IV plot is 21 and the RSE/EEE ratio using the error of 0.00085 A is 0.977. The measured max power of the TEG is 0.000287 W and the measured max power of the PV element is 0.182 W.*

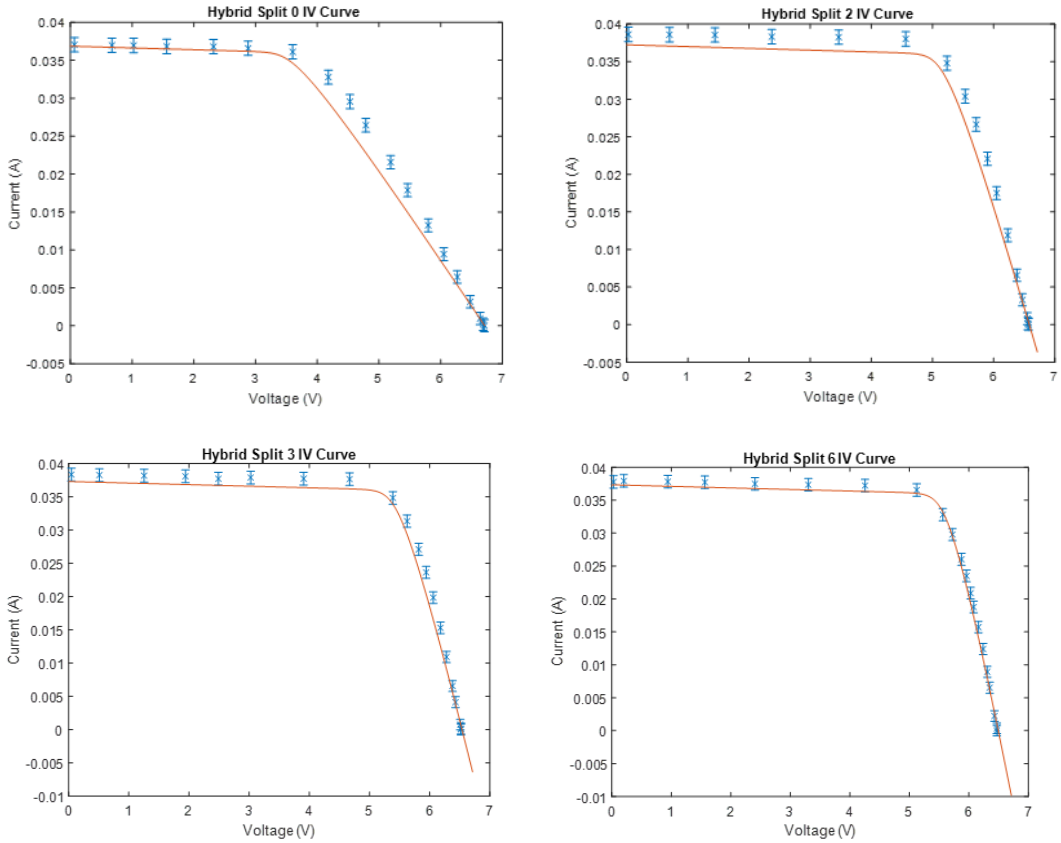

Figure 5.11: *Run 3 data points for PV/TEG series hybrid with no splitting, splitting level 2, splitting level 3, and splitting level 6. The current experimental error is 0.00085 A as previously stated. The solid lines*

are the expected current values predicted by the circuit model. The RSE/EEE ratios are 5.790, 7.621, 4.689, and 1.498 respectively. The number of data points in each plot are 19, 17, 20, and 21 respectively.

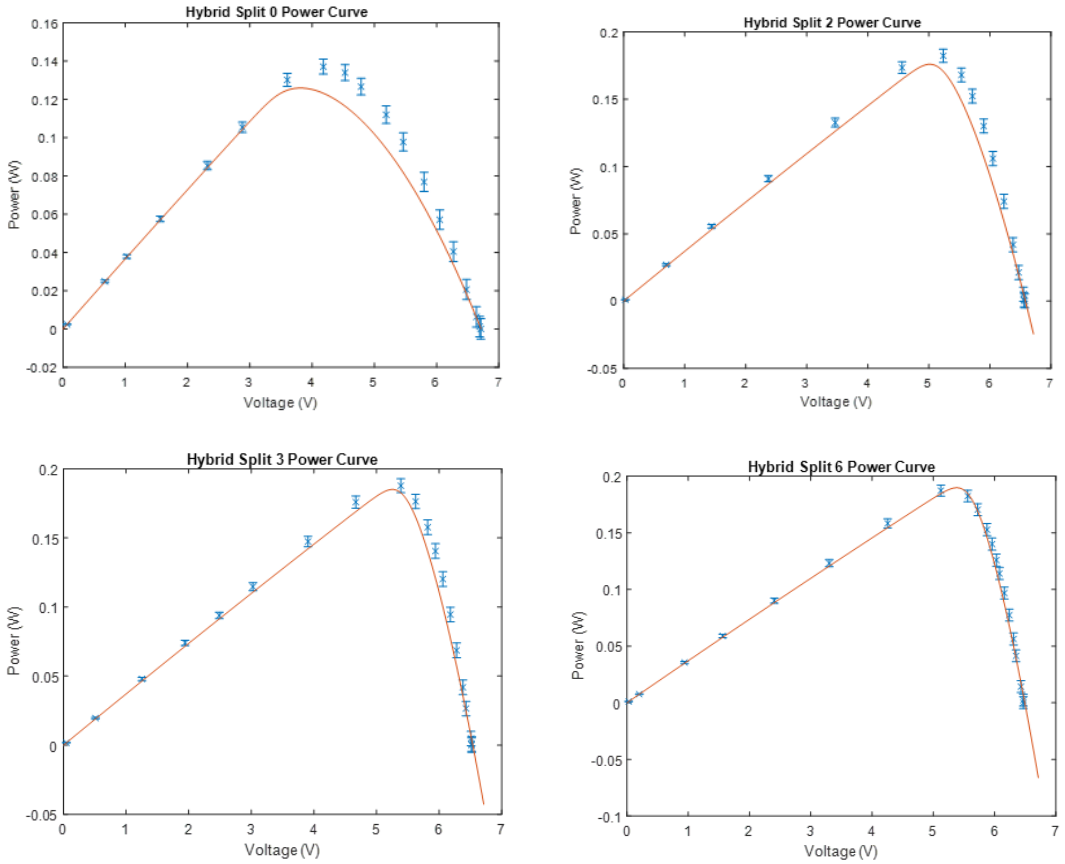

Figure 5.12: *Run 3 power curves for PV/TEG series hybrid with no splitting, splitting level 2, splitting level 3, and splitting level 6. The error of each point is the current error (0.00085 A) multiplied by the voltage. The solid lines are the power curves predicted by the circuit model. The lowest power measurement error is 0.0000258 W and the largest is 0.0054 W.*

	(1,2,3,4,5,6)	*(1,2,3)*	*(4,5,6)*	*(1,2)*	*(3,4)*	*(5,6)*
Voltage	0.265 V	0.105 V	0.157 V	0.0644 V	0.0845 V	0.109 V
Resistance	61.73 Ω	20.28 Ω	31.45 Ω	14.31 Ω	11.74 Ω	32.154 Ω

	(1)	*(2)*	*(3)*	*(4)*	*(5)*	*(6)*
Voltage	0.031 V	0.0317 V	0.0376 V	0.0459 V	0.0753 V	0.0359 V
Resistance	6.083 Ω	10.24 Ω	6.485 Ω	6.557 Ω	23.53 Ω	6.536 Ω
Temperature	40.7 °C	40.1 °C	43.7 °C	44.1 °C	46.5 °C	38.9 °C

Table 5.3: *Run 3 sub-TEG voltage and resistance values. (1,2,3,4,5,6) corresponds to the unsplit TEG, (1,2,3) and (4,5,6) correspond to the sub-TEGs for the splitting level of 2, and so forth. The surface temperatures of each TEG/PV module are also listed.*

5.8 Run 4 Data

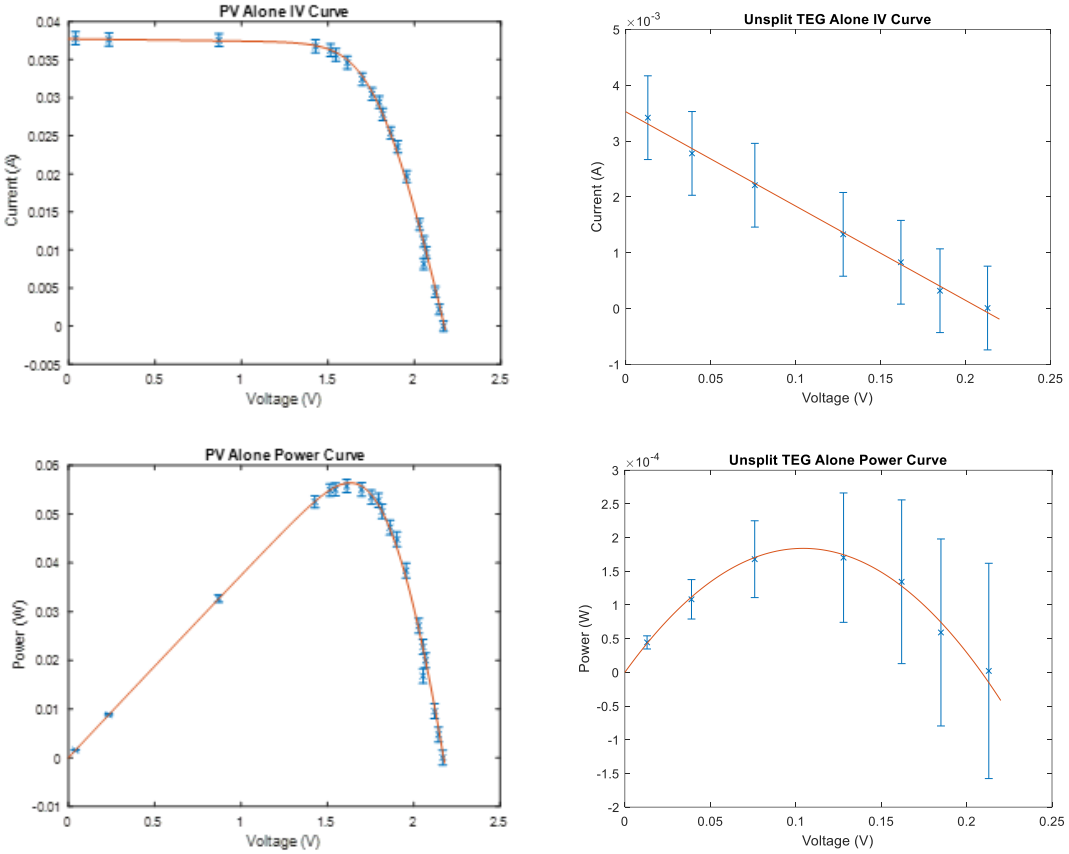

Figure 5.13: *Run 4 IV and power data points for PV element alone and unsplit TEG alone. The experimental error in the current was estimated to be 0.00075 A using the method described above. The error in the power data points is the voltage multiplied by the current error. The solid line curve in the PV element plot is the single diode model for parameters that best fit the data points. The solid line in the TEG plot is the least squares fit line for the data points. The number of data points in the PV IV plot is 21 and the RSE/EEE ratio using the error of 0.00075 A is 0.994. The measured max power of the TEG is 0.000170 W and the measured max power of the PV element is 0.0558 W.*

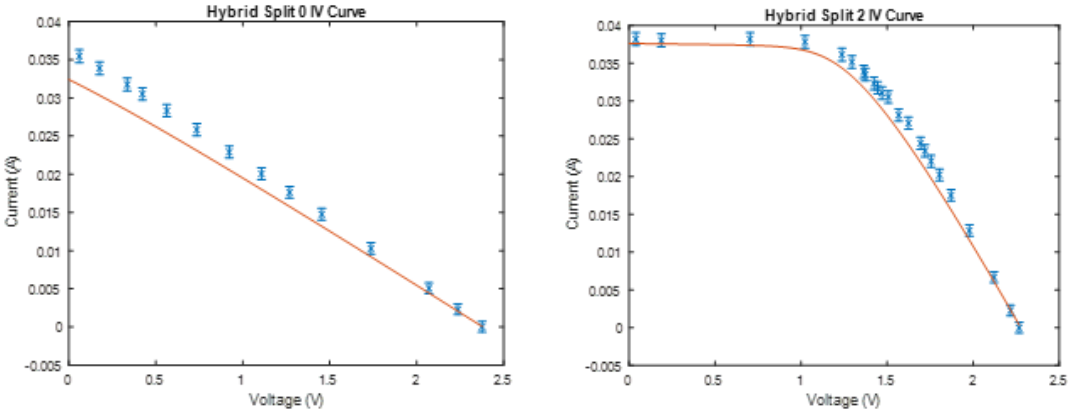

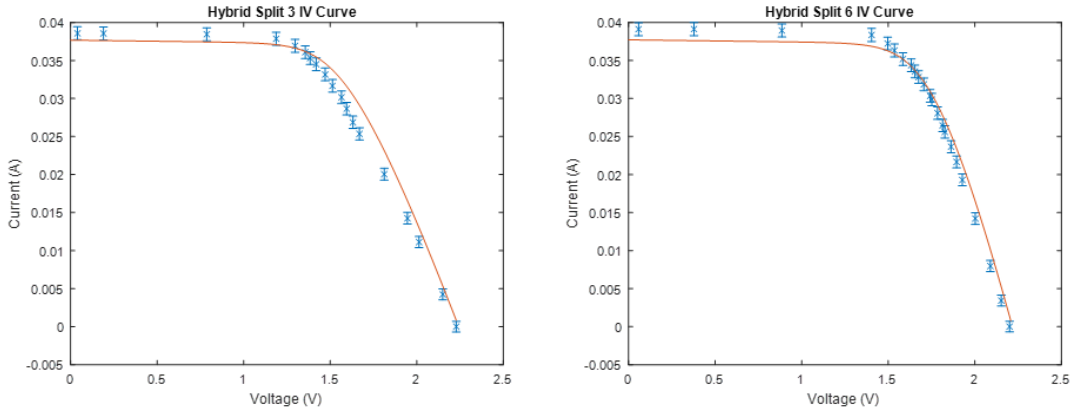

Figure 5.14: *Run 4 data points for PV/TEG series hybrid with no splitting, splitting level 2, splitting level 3, and splitting level 6. The current experimental error is 0.00075 A as previously stated. The solid lines are the expected current values predicted by the circuit model. The RSE/EEE ratios are 12.207, 6.623, 7.427, and 2.005 respectively. The number of data points in each plot are 14, 23, 19, and 23 respectively.*

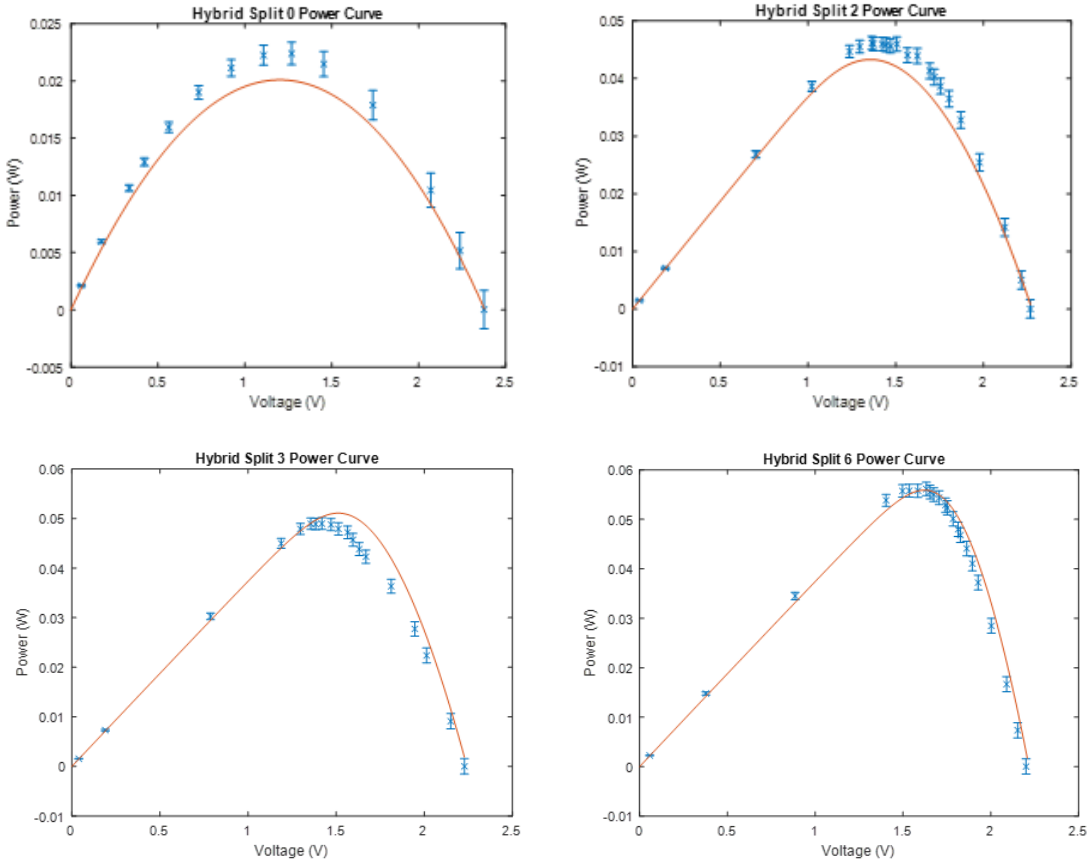

Figure 5.15: *Run 4 power curves for PV/TEG series hybrid with no splitting, splitting level 2, splitting level 3, and splitting level 6. The error of each point is the current error (0.00075 A) multiplied by the voltage. The solid lines are the power curves predicted by the circuit model. The lowest power measurement error is 0.0000333 W and the largest is 0.0017 W.*

	(1,2,3,4,5,6)	(1,2,3)	(4,5,6)	(1,2)	(3,4)	(5,6)
Voltage	0.2071 V	0.08154 V	0.13287 V	0.05506 V	0.054087 V	0.09697 V
Resistance	59.1716 Ω	21.459 Ω	34.965 Ω	17.762 Ω	12.019 Ω	30.303 Ω

	(1)	(2)	(3)	(4)	(5)	(6)
Voltage	0.03164 V	0.02262 V	0.02147 V	0.03048 V	0.06075 V	0.037606 V
Resistance	8.326 Ω	11.9048 Ω	8.258 Ω	8.4674 Ω	23.3645 Ω	7.6746 Ω
Temperature	37.3 °C	34.9 °C	34.1 °C	39.7 °C	41.3 °C	41.9 °C

Table 5.4: *Run 4 sub-TEG voltage and resistance values. (1,2,3,4,5,6) corresponds to the unsplit TEG, (1,2,3) and (4,5,6) correspond to the sub-TEGs for the splitting level of 2, and so forth. The surface temperatures of each TEG/PV module are also listed.*

5.9 Experimental Results

It can be seen from the chi squared values that the circuit model and data points were not a good fit for most of the IV curves. The only hybrid device IV curves that had statistically good fits were the no split and level 3 split hybrid devices for Run 2. It should also be noted that the other hybrid IV curves for this run were very close to having a good fit.

It can also be seen from the resistance and voltage values of the sub-TEGs for each run that even splitting of the TEGs was not achieved in the experimental setup. Since the model assumes that the TEG splitting is done evenly, it is understandable that the models may not match well to the measured data.

Runs 1 and 2 both used the same number of solar cell modules in series for the PV element but had quite different results in that Run 1 had a very poor fit to the model while Run 2 had an almost good fit to the model. It is tempting to explain this by reasoning that the grid configuration of Run 1 would lead to greater differences in temperature conditions on the sub-TEGs than the circular configuration of Run 2. However, looking at the sub-TEG values (Tables 1 and 2), it can be seen that the differences between the sub-TEGs are very similar in both runs.

The second noticeable difference between these two runs is the significance of the TEG power. Run 2 had the light source at a greater distance from the device, so the TEG did not get as hot. Because of this, the TEG power is 0.17% of the PV element power for Run 1 and 0.042% for Run 2. It seems that the less contribution the TEG power provides, the better the circuit model fits the data.

This trend continues into Runs 3 and 4. These runs have very similar differences in temperature conditions to Runs 1 and 2, but they use less solar cell modules, which makes the TEG a more significant contribution to the power. In Run 3, the TEG provides 0.16% of the PV element power and in Run 4 it provides 0.30%. Run 4 has the worst fit and Run 3 is comparable to Run 1.

In addition, the fit seems to increase as the splitting level of the TEG increases and the curve becomes more similar to the PV element IV curve. All of this points towards the overall trend being that, as the hybrid device's IV curve gets more distorted from that of the PV element's IV curve, the model gets less accurate. However, upon visual inspection the model does not seem to fail totally. In each IV curve, the model seems to do a fairly good job at predicting the shape of the measured IV curve. It is just shifted off of the measured values leading to a poor fit between the two.

From the data, it can be seen that the method of splitting the TEG does improve the fill factor and increases the max power of the hybrid device. This is most noticeable in Run 4 as the unsplit hybrid device has a very poor fill factor. It can also be seen in the data that the fill factor degradation from the TEG becomes less significant as the TEG's power contribution becomes less significant, which was also observed for the circuit model.

One last thing to notice is that the TEG power contribution for each run was less than 1% of the PV element power and was between the highest and lowest values for the power measurement error. Because of this, the TEG power is not conclusively distinguishable from power measurement error and it is not possible from this experimental setup to measure if the TEG power is being added to the PV element power for any of the hybrid scenarios.

Chapter 6: Conclusion

Chapter 6 presents a discussion of the results from the modeling and experimental work presented in chapters 4 and 5 respectively. Recommendations for future research are also discussed.

6.1 Modeling Results Discussion

The circuit model that was developed for the PV/TEG series connected hybrid device with TEG splitting showed empirical evidence that for any set of circuit model parameters, there exists some splitting level that results in lossless combination of the PV element and TEG max powers. This would mean that the power of the PV element and TEG element can be electrically combined without loss in general. In my opinion, this is the most important result of this work.

Being able to electrically combine the PV element and TEG without loss is very important for the application of PV/TEG hybrid devices. The method of splitting the TEG to achieve lossless electrical combination of the two elements is more practical than the method of changing the temperature gradient across the TEG, which was presented in prior research.

An additional result of interest from the modeling was that the fill factor degradation in the PV/TEG series connected hybrid depended on the significance of the power contribution of the TEG. That is, when the max power of the TEG is a large percentage of the PV element max power, the fill factor degradation is significant. When it is a low percentage, the degradation is less significant.

The fill factor degradation is caused by the TEG resistance being added to the PV series resistance. The PV element power can be increased by altering model parameters other than the series resistance. So, without changing either the PV series resistance or the TEG resistance, the fill factor degradation can be decreased simply by increasing the power contribution of the PV element. To me, this is not an obvious result which makes it interesting.

6.2 Experimental Results Discussion

The main purpose of the experimental section of this work was to see if the circuit model developed for the PV/TEG series connected hybrid device with TEG splitting would accurately predict the measured values from an experimental device. According to the statistical analysis of the data, the measurements and the model predictions did not match well.

One possible explanation for this is the uneven splitting of the TEG. The data showed that the sub-TEGs from the splitting had significant variation in their voltage and resistance values. This means that the splitting of the TEG in the experimental device was not even. Even splitting of the TEG is one of the assumptions that the circuit model assumes. However, this does not apply for the no split case of the hybrid device which was also found to have poor matching between the measurements and model.

I think a better explanation for the poor matching between the measurements and model is the effects of mismatch in current between the PV element and TEG. Prior research has shown that electrically connecting TEGs with mismatch current in series can cause effects in the TEG performance [9]. The circuit model developed for the hybrid TEG/PV series connection does not consider any effects from current mismatch between the PV element and the TEG.

Additionally, it was observed that the match between the measurements and model generally improved as the splitting level of the TEG was increased. As the splitting level increases, the portion of the PV element current going through an individual sub-TEG decreases and the mismatch between the PV element current and sub-TEG current may be decreased. This fits in with the idea that current mismatch effects were a cause of the poor fit of the model.

6.3 Suggestions for Future Research

A good next step for future research would be to obtain conclusive experimental evidence for the accuracy or inaccuracy of the hybrid device circuit model. A more sophisticated experimental setup that can split the TEG in a relatively even way would be useful for this. Additionally, the effects of the current mismatch between the PV element and TEG in this device architecture should be studied. It may be possible to do this with a theoretical approach, but most likely experimental methods would be needed to accurately understand the current mismatch effects.

It would also be important to create a hybrid device that achieves electrical combination of the PV element power and TEG power that is close to the lossless condition that occurs in the circuit model. The experimental setup in this work could not investigate this because the TEG power was too small to be distinguishable from measurement error in the hybrid device power. As more efficient thermoelectric materials become available, it should be possible to create an experimental setup where the TEG power is much larger than any error in the measurement. For this setup, it will be possible to conclusively measure how the TEG power and PV element power are being combined in the hybrid device and hopefully something close to the lossless condition can actually be achieved in a real device.

One issue with the application of the TEG split method is that the optimal splitting level is only optimal for some window of the circuit model parameters. In a real device, the environmental conditions will change and the circuit model parameters of the PV element and TEG will change along with them. However, the splitting level of the TEG will stay the same as this is a characteristic of the device's construction.

If the environmental conditions change enough that the current splitting level is no longer optimal, the device will no longer be operating with the lossless combination of the PV element and TEG. It would be good to investigate what kind of windows of optimal performance are possible with this type of device.

Bibliography

[1] D. Champier, "Thermoelectric generators: A review of applications". *Energy Conversion and Management*, vol. 140, pp. 167-181, DOI:10.1016/j.enconman.201702070, (2017).

[2] H. Chen, N. Wang, H. He, "Equivalent circuit analysis of photovoltaic-thermoelectric hybrid device with different TE module structure". *Advances in condensed Matter Physics*, vol. 2014, no. 824038, 2014.

[3] H.J. Goldsmid, "Introduction to Thermoelectricity", Second Edition. Springer, New York (NY), 2016.

[4] R. He, G. Schierning, K. Nielsch, "Thermoelectric Devices: A Review of Devices, Architectures, and Contact Optimization". *Advanced Materials Technologies*, vol. 3, no. 1700256, DOI:10.1002/admt.201700256, (2018).

[5] T.H. Kwan, X. Wu, "TEG Maximum Power Point Tracking Using an Adaptive Duty Cycle Scaling Algorithm". *Energy Procedia*, vol. 105, pp. 14-27, DOI:10.1016/j.egypro.201703274, (2017).

[6] D. Li, Y. Gong, Y. Chen, J. Lin, Q. Kahn, Y. Zhang, Y. Li, H. Zhang, H. Xie, "Recent progress of two-dimensional thermoelectric materials". *Nano-Micro Letters*, vol. 12, no. 36, DOI:10.1007/s40820.0200374, (2020).

[7] B. Lorenzi, M. Acciarri, D. Narducci, "Suitability of Electrical Coupling in Solar Cell Thermoelectric Hybridization". *Designs*, vol. 2, no. 32, DOI:10.3390/designs2030032, (2018).

[8] McCormick School of Engineering, "A Brief History of Thermoelectrics". *Northwestern University*, (2022). Available: History of Thermoelectrics (northwestern.edu)

[9] A. Montecucco, J. Siviter, A.R. Knox, "The effect of temperature mismatch on thermoelectric generators electrically connected in series and parallel". *Applied Energy*, vol. 123, pp. 47-54, DOI:10.1016/j.apenergy.201402030, (2014).

[10] N. Mughees, "Thermoelectric power generators for wearable electronics". *Electronics360*, September 9, (2021). Available: Thermoelectric power generators for wearable electronics | Electronics360 (globalspec.com)

[11] nanohubtechtalks, "Introduction to Thermoelectricity L1.1 – L1.7". YouTube, October 21, (2019). Available: Introduction to Thermoelectricity L1.1: Theory - Introduction - YouTube

[12] D. Narducci, P. Bermel, B. Lorenzi, N. Wang, K. Yazawa, "Hybrid and Fully Thermoelectric Solar Harvesting". Springer, New York (NY), 2018.

[13] K. Park, S. Shin, A.S. Tazebay, H. Um, J. Jung, S. Jee, M. Oh, S. Park, B. Yoo, C. Yu, J. Lee, "Lossless hybridization between photovoltaic and thermoelectric devices". *Scientific Reports*, vol. 3, no. 2123, DOI:10.1038/srep02123, (2013).

[14] P.D. Raut, V.V. Shukla, S.S. Joshi, "Recent developments in photovoltaic-thermoelectric combined system". *International Journal of Engineering & Technology*, vol. 7, no. 4, pp. 2619-2627, DOI: 10.14419/ijet.v7i4.12709, (2018).

[15] J. Richard, "How to Build a Homemade Thermoelectric Generator". *TopMagneticGenerator.com*, March 13, (2021). Available: How to Build a Homemade Thermoelectric Generator (topmagneticgenerator.com)

[16] A.Z. Sahin, K.G. Ismaila, B.S. Yilbas, A. Al-Sharafi, “A review on the performance of photovoltaic/thermoelectric hybrid generators”. *International Journal of Energy*, vol. 44, pp. 3365-3394, DOI:10.1002/er.5139, (2020).

[17] S. Shittu, G. Li, X. Zhao, X. Ma, “Review of thermoelectric geometry and structure optimization for performance enhancement”. *Applied Energy*, vol. 268, no. 115075, DOI:10.1016/j.apenergy.2020115075, (2020).

[18] S. Siouane, S. Jovanovic, P. Poure, “Equivalent Electrical Circuits of Thermoelectric Generators under Different Operating Conditions”. *Energies*, vol. 10, no. 386, DOI:10.3390/en10030386, (2017).

[19] A. Smets, K. Jager, O. Isabella, R.V. Swaaij, M. Zeman, “Solar Energy”. UIT Cambridge Ltd, Cambridge England, 2016.

[20] P. Sundarraj, D. Maity, S.S. Roy, R.A. Taylor, “Recent advances in thermoelectric materials and solar thermoelectric generators – a critical review”. *Royal Society of Chemistry Advances,* vol. 4, pp. 46860-46874, DOI:10.1039/c4ra05322b, (2014).

[21] R. Thankakan, E. Rajan, S. Nadar, “Investigation of thermoelectric generators connected in different configurations for micro-grid applications”, *International Journal of Energy Research*, vol. 42, pp. 2290-2301, DOI:10.1002/er.4015, (2018).

[22] N. Wang, L. Han, H. He, N. Park, K. Koumoto, “A novel high-performance photovoltaic-thermoelectric hybrid device”. *Energy and Environmental Science*, vol. 4, pp. 3676-3679, DOI:10.1039/clee01646f, (2011).

[23] L. Xu, Y. Xiong, A. Mei, Y. Hu, Y. Rong, Y. Zhou, B. Hu, H. Han, “Efficient perovskite photovoltaic-thermoelectric hybrid device”. *Adv. Energy Mater*, vol. 8, no. 1702937, DOI:10.1002/aenm.201702937, (2018).

[24] H. Yang, F. Kang, C. Ding, J. Li, J. Kim, D. Baek, S. Nazarian, X. Lin, P. Bogdan, N. Chang, "Prediction-based fast thermoelectric generator reconfiguration for energy harvesting from vehicle radiators", 2018 Design. *Automation & Test in Europe Conference & Exhibition*, 2018, pp. 877-880, DOI: 10.23919/DATE.2018.8342130.

[25] J. Zhang, Y. Xuan, “The electric feature synergy in the photovoltaic – thermoelectric hybrid system”. *Energy*, vol. 181, pp. 387-394, DOI:10.1016/j.energy.201905155, (2019).